

Higher-Order Tails and RG Flows due to Scattering of Gravitational Radiation from Binary Inspirals

Alex Edison ^a, Michèle Levi^b

^a*Department of Physics and Astronomy, Northwestern University, Evanston, Illinois, 60208, USA*

^b*Mathematical Institute, University of Oxford, Oxford OX2 6GG, United Kingdom*

E-mail: alexander.edison@northwestern.edu, levi@maths.ox.ac.uk

ABSTRACT: We establish and develop a novel methodology to treat higher-order non-linear effects of gravitational radiation that is scattered from binary inspirals, which employs modern scattering-amplitudes methods on the effective picture of the binary as a composite particle. We spell out our procedure to study such effects: assembling tree amplitudes via generalized-unitarity methods and employing the closed-time-path formalism to derive the causal effective actions, which encompass the full conservative and dissipative dynamics. We push through to a new state of the art for these higher-order effects, up to the third subleading tail effect, at order G_N^5 and the 5-loop level, which corresponds to the 8.5PN order. We formulate the consequent dissipated energy for these higher-order corrections, and carry out a renormalization analysis, where we uncover new subleading RG flow of the quadrupole coupling. For all higher-order tail effects we find perfect agreement with partial observable results in PN and self-force theories, where available.

Contents

1	Introduction	2
2	EFT of Binary as Composite Particle	4
2.1	Closed-Time-Path Formalism	6
3	Amplitudes and Generalized Unitarity	7
3.1	Tree Amplitudes	8
3.2	Generalized Unitarity Cuts	9
4	The Tail Effect	11
4.1	Building Blocks	13
4.2	Radiation-Reaction	15
4.3	Tail	18
5	Higher-Order Tails	21
5.1	Tail-of-Tail	21
5.2	Tail-of-Tail-of-Tail	25
5.3	Tail-of-Tail-of-Tail-of-Tail	27
6	Analysis of Dissipative Sector	31
6.1	Energy Loss in the CTP Formalism	31
6.2	Radiated Energy from Tails	33
6.3	Going to Subleading RG Flow	34
7	Post-Newtonian and Self-Force Results	37
7.1	PN Mapping to the Binary Inspiral	37
7.2	Direct Comparisons	38
8	Conclusions	40
A	Handling Tensor Reductions	41
B	Evaluating Basis Integrals	42
B.1	Analytic Evaluation and Bubble Iteration	42
B.2	Evaluation of Figure 8h	44

1 Introduction

The direct observation of gravitational waves (GWs) coming from binary black hole (BBH) merger events [1–6] has shifted precision predictions of GW and BBH structure from theoretical curiosity to phenomenological imperative. With four gravitational-wave observatories active through the LIGO-VIRGO-KAGRA network [7–9] and new ground- and space-based detectors on the way [10–12], the increasing scope and depth of incoming gravitational-wave data threatens to exceed our currently available predictions. To meet this looming demand, the last few decades have seen an explosive growth on the theoretical frontier.

The longest-running framework for studying GW sources during the significant inspiral phase is post-Newtonian (PN) General Relativity, which deals with simultaneously weakly interacting and slowly moving bodies; we refer the interested reader to Ref. [13] for a comprehensive Living Review on the subject. With both the orbital velocity and the gravitational coupling as small parameters, PN computations build on classical two-body Newtonian dynamics, and compute the perturbative corrections in these small parameters induced by GR (hence the “post-Newtonian” moniker). Note that the PN approximation treats the perturbation constants as $G_N \sim v^2/c^2 \ll 1$, and thus admits half-PN counting through single powers of v . Due to the long-standing unique prominence of inspiraling binaries as GW sources, PN calculations have been the primary basis for the generation of theoretical gravitational waveforms.

The state of the art in PN theory is currently focused on the 5, 5.5, and 6PN order via multiple approaches, including traditional GR methods [14–16], as well as particle-physics inspired [17] effective field theory (EFT) methods using Feynman technology [18–20]. Starting at 2.5PN, radiative effects become essential. The leading dissipative contribution, originally derived by Einstein, and later by Burke and Throne [21–23], has come to be known as the “radiation-reaction” term. As of 4PN, the system dynamics must also account for a collection of phenomena known as “tail” effects, in which radiation from the system scatters off of the system’s own potential background [24, 25]. The leading tail effect has also been well-studied in the EFT context [26–29]. On the other hand, the subleading “tail-of-tail” has received limited direct study [26, 30], and the sub-subleading “tail-of-tail-of-tail” (T^3) has only been computed via traditional GR methods [31], without a counterpart EFT computation.

It is also possible to release the small-velocity approximation used in the PN expansion, and work instead with Special Relativity as the base theory on top of which gravitational sources produce small fluctuations, with G_N serving as the only perturbation parameter. This aptly named “post-Minkowskian” (PM) approximation has seen a surge of interest in recent years, thanks in part to the close similarity between gravitational-wave source calculations in PM and computing effective potentials via scattering amplitudes [32]. The state of the art in PM calculations has recently been pushed to 4PM [33–40], and is currently one of the driving forces in understanding certain classes of Feynman integrals. Even though these computations are carried out in the scattering regime, there are methods for extracting quantities relevant to the bound problem from them [32, 41–45]. However, these

mappings between the bound and scattering regimes are expected to break down beyond 4PM as a result of the nonlocal-in-time contributions coming from the tails and similar higher-order effects [24, 25, 43, 46].

Thus, the study of tail effects is critical both for their direct relevance to the real-world PN sources, as well being a key piece for possibly understanding the connection between bound and unbound systems. This work extends and pushes our study of higher-order tail effects by building on our previous letter, Ref. [47]. In that paper, we briefly introduced a novel approach to calculating higher-order tail effects by exploiting generalized unitarity methods [48–51]. Using this approach, we were able to compute the quadrupole-sourced tail effects up through T^3 at G^4 , which matched state-of-the-art results from traditional GR methods [31], and surpassed previous attempts using EFT techniques [26–29]. In this work, we provide a significantly more detailed discussion of the new methodology, including laying out the constituent building-block amplitudes, as well as in-depth calculations through the tail-of-tail. As further novel results of this work, we calculate through to the tail-of-tail-of-tail (T^4) contribution at G^5 to the quadrupole-quadrupole effective action, eq. (5.32), and energy dissipation, eqs. (6.18) and (6.31). With the new energy-loss term, we are able to compute new subleading RG flow of the quadrupole source, eq. (6.33), extending the results of Refs. [26, 52] to further allow for prediction of all *subleading* logs in tail-induced energy-loss.

The structure of this paper is as follows. In the next couple of sections, we provide a somewhat disjoint review of relevant material of EFT and Amplitudes methods for our hybrid approach to the computation of tail effects. In section 2, we focus on the EFT setup for the tails problem. We discuss the relevant separation of scales and the emergence of tails as a phenomena that signals the breakdown of this separation. In section 2.1 we lay out the closed-time-path (CTP) formalism adapted by Galley et al [53, 54], from QFT to our classical context as a method of computing dissipative effective actions. Subsequently, in section 3 we present some of the basic results and modern methods common in the study of scattering amplitudes, and point out how they will be of use for the computation of tails.

Sections 4 and 5 contain the heart of this paper. In section 4 we elaborate on the elements of our novel methodology, and demonstrate it on the leading radiation-reaction and tail effects, which have been well-studied in terms of effective actions. In section 5, we proceed to present the computation of new effective actions of higher-order tails up through T^4 , the first ever computation of this effect, using generalized unitarity methods. We relegate details about integration to the appendices A and B. In section 6, we first formulate the energy loss through the use of the CTP approach for the binary inspiral, and we explicitly extract the related contributions to the radiated energy. With this collection of dissipation corrections in hand, we proceed to analyze them to determine the renormalization and RG flow of the quadrupole source, finding agreement with previous leading EFT results [26, 27], and extending the RG flow to subleading order. Finally, in section 7 we cross-check our new higher-order results against partial ones, known from PN and self-force theory, where they overlap [31, 55, 56], and find perfect agreement.

2 EFT of Binary as Composite Particle

The effective field theory description of binary inspirals in PN gravity has been formally defined since Goldberger and Rothstein's seminal work [17]. We briefly review it here. We direct interested readers to Refs. [57, 58] for more recent comprehensive reviews of the subject.

Starting from the binary PN assumptions of small velocity and weak field, the two constituent massive objects have *non-relativistic* momenta given by

$$p_i^\mu \sim (m_i v^2, m_i v) \quad (2.1)$$

governed by two small quantities, approximately equated by the virial theorem,

$$v^2 \sim \frac{G_N m}{r} \ll 1, \quad (2.2)$$

with m the characteristic mass of the gravitating particles, r their orbital separation, and v their characteristic orbital velocity. The gravitational field due to the interaction between the two inspiraling bodies can then be split into two graviton modes:

$$k^\mu \sim \begin{cases} (v/r, 1/r) & \text{potential (near zone)} \\ (v/r, v/r) & \text{radiation (far zone)} \end{cases}, \quad (2.3)$$

and the recoil from each of the massive bodies interacting with the gravitons is assumed to be negligible, which allows to handle the components as classical sources on non-dynamical worldlines. The momentum of the potential modes has a dominant spatial component, and thus they are treated as space-like instantaneous mediators. As their name suggests, these modes are responsible for the gravitational binding of the two-body system. From these considerations, a full effective action at the orbital scale was defined in Ref. [17] with manifest power-counting following eq. (2.2). This effective action has been used extensively for computations of the binding energy of gravitational binaries, and even extended to include spin-induced effects of the binary [59–84].

Beyond the orbital-scale conservative sector, namely when radiation modes also participate in interactions, it is beneficial to consider as a starting point the entire binary system as a single point particle moving on a worldline, with its internal structure modeled by multipole moments coupled to gravity. This effective action of the binary as a composite particle, which is analogous to that of the single compact object with its spin-induced multipoles at the orbital scale, is given by [26, 58, 63, 68, 85]:

$$S_{\text{eff}(c)}[g_{\mu\nu}, y_c^\mu, e_{cA}^\mu] = -\frac{1}{16\pi G} \int d^4x \sqrt{g} R[g_{\mu\nu}] + S_{\text{pp}(c)}[g_{\mu\nu}(y_c), y_c^\mu, e_{cA}^\mu](\sigma_c), \quad (2.4)$$

with

$$S_{\text{pp}(c)}[h_{\mu\nu}, y_c^\mu, e_{cA}^\mu](t) = - \int dt \sqrt{g_{00}} \left[E(t) + \frac{1}{2} \epsilon_{ijk} L^k(t) \left(\Omega_{\text{LF}}^{ij} + \omega_\mu^{ij} u^\mu \right) - \sum_{l=2}^{\infty} \left(\frac{1}{l!} I^L(t) \nabla_{L-2} \mathcal{E}_{i_{l-1} i_l} - \frac{2l}{(l+1)!} J^L(t) \nabla_{L-2} \mathcal{B}_{i_{l-1} i_l} \right) \right] \quad (2.5)$$

in terms of the time coordinate t as the composite-particle worldline parameter. The point-particle action includes gravitational couplings to the particle’s total energy $E(t)$, its angular momentum $L^k(t)$, and higher multipoles of charge and current type with definite parity, $I^L(t)$ and $J^L(t)$ respectively, bearing symmetric traceless SO(3) (spatial Euclidean) tensor indices. \mathcal{E} and \mathcal{B} are the respective even- and odd-parity components of the gravitational curvature tensor¹. In the current work, we limit ourselves to the leading (static) gravitating energy, $E(t) \rightarrow E + \mathcal{O}(G_N)$, ignoring various subleading corrections due to the gravitational interactions.

Since gravity is self-interacting, integrating out the gravitational field, starting from this EFT of the composite particle, will involve fully analyzing interactions that include both potential and radiation modes, as the separation of scales inevitably breaks down at a sufficiently high perturbative order of the EFT. The simplest class of such effects is the scattering of a radiation-mode graviton with one or more potential-mode gravitons. The interaction with a single potential mode is referred to as the “tail” effect. We refer to interactions with n potential modes as (tail-of-) $n-1$ tail or T^n for brevity².

Successive terms in the multipole expansion carry increasing powers of radiation-mode momenta. As such, the tails related with each of these multipole sources enter at staggered orders in perturbation theory. In this work we analyze effects that are sourced only by quadrupoles, which yield the leading PN contributions in growing orders of the gravitational coupling constant, G_N . As we will see below, the analysis of this EFT of the composite particle at the radiation scale requires regularizing and renormalizing ultraviolet divergences. One can simply follow the standard method to handle renormalization in an EFT by introducing renormalized couplings, which means in this case modifying the coefficients of the multipole source terms to absorb the divergences. Matching with the orbital-scale EFT would align such ultraviolet divergences with infrared divergences in the small-scale theory.

Two approaches to addressing the tails have been presented in the literature. The first we refer to as the “one-point” formalism, which was used by Goldberger and Ross to construct the gravitational radiation from the tail and tail-of-tail [26]. In this setup, one computes the graviton one-point amplitude, $\mathcal{A}_h(k^\mu) \sim \varepsilon_{ij}(k^\mu)I^{ij}(k^0)$, with the (Fourier transform of the) quadrupole, $I^{ij}(\omega)$, as a classical source. From the one-point amplitude it is simple to construct a graviton differential emission rate, which can then be appropriately weighted and integrated to extract radiation effects, for instance the radiated four-momentum. This approach is elegant and well-motivated physically when all one desires is extracting dissipative features. However, it is ill-suited for extracting the effect on the *conservative dynamics* of the binary induced by the tails, which are of phenomenological import [14, 15, 19, 20, 27, 57, 58, 86].

The other approach, in which we base the current work and which does also account for the conservative dynamics, computes the effective “two-point function” of the

¹ Ω_{LF} is the generalized angular velocity in the local frame, and ω the Ricci rotation coefficient or spin connection, though they will not be relevant to the present work.

²Note that the nomenclature used by Blanchet [13, 30] makes a distinction between, for instance, tail² and tail-of-tail. In our EFT approach it is not particularly useful to make such a distinction.

quadrupole on the worldline that results from *integrating out* gravitational interactions with the quadrupole source. In this picture we can consider the gravitational field integrated out as an inaccessible degree of freedom, from which the quadrupole can gain or lose energy. The final result will be an effective action which takes the following form in frequency domain:

$$S^{\text{eff}} = \int d\omega f(\omega) I^{ij}(\omega) I_{ij}(-\omega), \quad (2.6)$$

where the shorthand $\kappa(\omega) \equiv I^{ij}(\omega) I_{ij}(-\omega)$ will be useful [87]. Because the result is an effective action for the evolution of a quadrupole, we have access to both the conservative dynamics through a Lagrangian, and to radiative observables, via some generalized calculus of variations within the Closed-Time-Path (CTP) formalism, see the following section 2.1 and later section 6.1. This CTP approach was put forward and popularized by Galley et al, starting in [88], and has since been adopted as the standard approach in EFT computations of tails [27, 29, 89–91]. Prior to our recent letter [47], there had been no attempt to use this approach to tackle higher-order (and unknown) tails.

2.1 Closed-Time-Path Formalism

The nonconservative sector requires a more intricate treatment since the radiating binary is in fact an open system as its leaking energy via gravitational waves, so time reversal no longer holds beyond the conservative sector. As we noted above, while specific setups can be used to model the radiative features of the binary [26], these still run into difficulties disentangling the causal radiation effects [52]. Over the last decade, it has become clear that care must be taken when handling the nonconservative effects present in inspiraling binaries [53, 54, 88, 89]. In fact, the approach detailed in Galley et al [54, 89] successfully dealt with radiation reaction and tails at the level of the effective action [27, 53, 88]. This approach is based on the closed-time-path (CTP) (or “in-in”) formalism [53, 54, 92, 93], and also fully accounts for the conservative effects due to tails.

The CTP approach adopted to our worldline EFT provides a classical method of integrating out the gravitational field degrees of freedom while maintaining time-asymmetry at the level of the resulting effective action. This is achieved by formally *doubling all degrees of freedom* in the initial full action of the system, and defining the initial CTP action as:

$$S_{\text{CTP}}[\{\dots\}_1, \{\dots\}_2] = S[\{\dots\}_1] - S^*[\{\dots\}_2], \quad (2.7)$$

where $\{\dots\}_i$ denotes the full set of degrees of freedom of the system, including all worldline degrees of freedom, and all the field modes which we plan on integrating out. After integrating out the field degrees of freedom, we will obtain a CTP effective action of the form:

$$S_{\text{CTP}}^{\text{eff}} = \int dt \left[L(\overline{\{\dots\}}_1, t) - L(\overline{\{\dots\}}_2, t) + K(\overline{\{\dots\}}_1, \overline{\{\dots\}}_2, t) \right] \quad (2.8)$$

where $\overline{\{\dots\}}_{1/2}$ are the remaining worldline degrees of freedom, L is identified as the *conservative* Lagrangian, and K represents the *nonconservative* potential. While the initial action does not contain such a history-mixing term, the process of integrating out some of

the degrees of freedom will produce an effective mixing contribution. Once we have obtained the effective action in terms of the doubled variables, we extract physical dynamics and observables by varying the action with respect to the $\overline{\{\dots\}}_1$ variables, e.g., and then taking the *physical limit* (PL), $[\overline{\{\dots\}}_1 - \overline{\{\dots\}}_2]|_{\text{PL}} \equiv 0$.

Prior to integrating out it is more useful to perform a change of variables to $\{\dots\}_+ \equiv [\overline{\{\dots\}}_1 + \overline{\{\dots\}}_2]/2$, and $\{\dots\}_- \equiv \overline{\{\dots\}}_1 - \overline{\{\dots\}}_2$, which leads to a modified propagator matrix:

$$G_{+-} = G_{\text{adv}}, \quad G_{-+} = G_{\text{ret}}; \quad G_{++} = G_{--} = 0, \quad (2.9)$$

where the scalar component of the graviton propagator is given by:

$$G_{\text{ret/adv}}(x - x') = \int \frac{d^D p}{(2\pi)^D} \frac{e^{-ip_\mu(x-x')^\mu}}{(p^0 \pm i0)^2 - |\vec{p}|^2} \quad (2.10)$$

in the mostly-minus metric convention, with $p_{\text{ret}}^0 \equiv p^0 + i0$ for retarded, $p_{\text{adv}}^0 \equiv p^0 - i0$ for advanced, and where $D \equiv d + 1$ with d the number of spatial dimensions of \vec{p} . In this basis, the conservative contribution to the resulting effective action in eq. (2.8) is identified as the part that is symmetric under $\overline{\{\dots\}}_+ \leftrightarrow \overline{\{\dots\}}_-$, while the remaining terms are identified as the nonconservative K . Observables in this basis are extracted by performing the calculus of variations with respect to the $\overline{\{\dots\}}_-$ variables, after which the physical limit $\overline{\{\dots\}}_+ \rightarrow \overline{\{\dots\}}_{\text{PL}}$, $\overline{\{\dots\}}_- \rightarrow 0$ is applied. In section 6.1 below, we will derive the dissipated energy in the CTP formalism, also specialized in particular to the case of tails in binary inspirals.

As discussed in section 2, the effective action due to tails, which amounts to a two-point function of the mass quadrupole, results from integrating out its coupling to the gravitational field. Carrying out this task in the CTP framework is rather straightforward [27, 88, 89]. First, we endow the quadrupoles with CTP labels, $I^{ij}(\omega) \rightarrow I_a^{ij}(\omega)$, $\kappa(\omega) \rightarrow \kappa_{ab}(\omega)$ (we use a, b for CTP indices, reserving Latin letters near i, j for space-like indices). Then we sum over the possible CTP labels for the two quadrupoles, while making consistent CTP label choices for the internal radiation-mode gravitons. In the case of tails, this consistent label choice amounts to having all radiation-mode propagators, G_{ab}^{rad} , aligned with the quadrupole labels, e.g.

$$I_-^{ij}(\omega) G_{-+}^{\text{rad}} G_{-+}^{\text{rad}} \dots I_+^{ij}(-\omega). \quad (2.11)$$

Because the CTP propagators address causal propagation and the potential-mode gravitons are taken to be instantaneous, we do not dress them with CTP labels.

3 Amplitudes and Generalized Unitarity

The study of scattering amplitudes via the unitarity paradigm has a long and storied history, and this work is not intended as a review of the field. Instead we mention a few specific points that are relevant for the work at hand, so that non-experts have a point of reference. For readers interested in more details, we refer to Refs. [94–97] as broad introductions to the subject. For discussions particularly centered on multi-loop unitarity methods, we refer the reader to Refs. [50, 98–106].

3.1 Tree Amplitudes

Tree amplitudes have a number of basic properties that nonetheless serve as focus points for their study. They are a description of *local* scattering interactions between *on-shell* external particles that are *gauge invariant* and obey *factorization* rules. By on-shell, we mean that all of the external particles have energy-momentum vectors obeying $p_i^2 = m_i^2$ where m_i is the particle's rest mass.

Amplitudes describing massless spin-1 particles are invariant under linearized gauge transformations, i.e. if we explicitly factor polarization vectors out of an amplitude, they will obey the Ward identity

$$\mathcal{A}_n = \mathcal{A}_{n \mu_1 \dots \mu_n} \prod \varepsilon_i^{\mu_i} \rightarrow p_i^{\mu_i} \mathcal{A}_{n \mu_1 \dots \mu_n} \prod_{j \neq i} \varepsilon_j^{\mu_j} = 0. \quad (3.1)$$

Amplitudes of massless spin-2 particles (gravitons) are invariant under linear diffeomorphisms, realized via

$$\mathcal{M}_n = \mathcal{M}_{n \mu_1 \nu_1 \dots \mu_n \nu_n} \prod \varepsilon_i^{\mu_i} \varepsilon_i^{\nu_i} \rightarrow p_i^{\mu_i} \varepsilon_i^{\nu_i} \mathcal{M}_{n \mu_1 \dots \mu_n} \prod_{j \neq i} \varepsilon_j^{\mu_j} \varepsilon_j^{\nu_j} = 0. \quad (3.2)$$

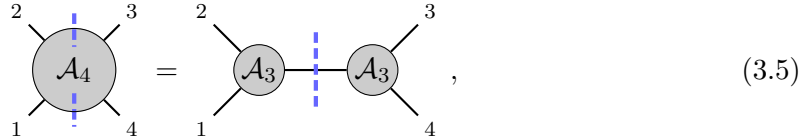
Here we have also introduced a standard notation for dealing with spin-2 amplitudes: since we require graviton polarizations to be symmetric traceless tensors we write them as an outer product of two identical null polarization vectors

$$\varepsilon^{\mu\nu} \rightarrow \varepsilon^\mu \varepsilon^\nu, \quad \varepsilon^\mu \varepsilon_\mu = 0. \quad (3.3)$$

Locality is the statement that the amplitude can be expressible in terms of point-like interactions, which in momentum space translates to only allowing interactions that are polynomials of momenta and polarizations. Similarly, factorization is a statement about the types of pole structures that appear in momentum space. Concretely, factorization requires that the residue of a momentum-space amplitude on a configuration where a sum of external momenta goes on-shell must be equal to a product of lower-point amplitudes summed over all theory-allowed intermediate on-shell states

$$\text{Res}_{(p_1 + \dots + p_j)^2 = 0} \mathcal{A}(1, \dots, j, j+1, \dots, n) = \sum_{\text{states of } i} \delta(p_i^2) \mathcal{A}(1, \dots, j, i) \mathcal{A}(i, j+1, \dots, n). \quad (3.4)$$

An example of the sum over graviton states is in eq. (3.10) below. Graphically, we often represent factorization as



$$\text{Diagram (3.5): } \mathcal{A}_4 = \mathcal{A}_3 \text{---} \mathcal{A}_3$$

where we used [dashed colored lines](#) in the diagram to highlight the cut internal legs. While it may seem like factorization is a direct consequence of locality, geometric constructions of amplitudes like the Amplituhedron [107] show that it is possible to manifest factorization without manifesting locality.

In addition to these standard properties, amplitudes involving non-Abelian charges, e.g. Yang–Mills theory, exhibit color-kinematics duality [103, 108]. The amplitudes in these theories can be written in terms of numerators dressing only cubic diagrams, where the kinematic piece of the numerators obeys the same algebraic relations as the non-Abelian color charge factors. These numerators can then be “double-copied” by replacing the color factors with another set of kinematic numerators, leading to amplitudes in uncolored theories. The most relevant example for the current work is that tree amplitudes for gravitational interactions, both self-interactions and coupling to matter, can be generated as the double-copy of Yang-Mills amplitudes, also potentially involving matter [103, 109, 110].

Over the years, different tree construction methods have been developed which manifest different properties of amplitudes. For instance, direct calculation via standard QFT Feynman rules manifests locality, factorization, and connection to path integrals and action principles, but obscures gauge invariance and relationships between theories. On the other hand, Britto-Cachazo-Feng-Witten recursion-based constructions [111–114] manifest gauge invariance, on-shell conditions, and high-energy behavior at the cost of no longer manifesting locality. Such recursion relations have been applied in studying candidates for “black hole + gravity” Compton amplitudes [115–118]. Of primary relevance to the current work is the Cachazo-He-Yuan formulation of scattering amplitudes [119, 120], which manifests the double-copy relations between gauge theory amplitudes and gravitational amplitudes at the cost of introducing an auxiliary space. One of the current authors and Fei Teng developed the publicly available package `IncreasingTrees` for efficiently computing gauge and gravity tree amplitudes, including minimal matter couplings, in this formalism [121]. Using it, we are able to extract all of the building-block amplitudes needed for the tail computations, which we discuss below in section 4.1.

3.2 Generalized Unitarity Cuts

The central concept of the unitarity program is the combining of tree amplitudes into loop data via *generalized unitarity cuts*. The core of generalized-unitarity methods comes from two connected ideas. First, through tensor reduction and integration relations [122–125], loop amplitudes can be written in terms of a basis of scalar integrals (and often purely-propagator integrands). When written in this basis, the coefficient of each basis integral is a theory-dependent algebraic function of the external data and spacetime dimension. Writing the amplitude in this way often exposes significant simplifications and patterns. An important and well-studied example is the four-point one-loop amplitude for any theory, which can be written as [122, 126–130]

$$\mathcal{A}_4^{(1)} = \text{Diagram} = c_{\text{box}} \int \text{Diagram} + c_{\text{s-bub}} \int \text{Diagram} + \text{perms} , \quad (3.6)$$

in which c_{box} , $c_{\text{s-bub}}$, and what is covered by “perms” are all theory dependent.

While expressing amplitudes in terms of scalar integral bases is a useful organizing principle on its own, its real power comes with the help of the second observation: the perturbative QFT optical theorem can be used to directly construct the basis coefficients c_i . The key idea, developed by Bern, Dixon, Dunbar, and Kosower (BDDK) [48, 49], is that unitarity of the S -matrix perturbatively requires

$$-i(T - T^\dagger) = T^\dagger T \Rightarrow 2 \operatorname{Im} \left(\text{Diagram of a loop with 4 external legs} \right) = \int \text{dLIPS} \left(\text{Diagram of two trees connected by a cut} \right), \quad (3.7)$$

where the two trees on the right hand side are fully on-shell amplitudes, dLIPS is the Lorentz invariant phase space measure encoding the loop integral measure and the on-shell cut conditions, and the \otimes instructs us to sum over all possible on-shell states crossing the cut and integrate over the on-shell phase space of the internal particles. We are limiting the drawing to four external particles in keeping with the example of eq. (3.6). This relation tells us that the branch cut structure of the integrated amplitude, probed by the left-hand side of the equality, is related to pole structures of tree amplitudes. BDDK demonstrated that careful repeated application of eq. (3.7) completely determines the integrated amplitude [48, 49].

Combination and refinement of these two ideas leads to relating the right hand side of eq. (3.7) with linear combinations of the integral basis coefficients [48–51]. The relations can be exploited algorithmically by not explicitly evaluating the $\int \text{dLIPS}$ in eq. (3.7), but instead using integration reduction to re-express the rational function of loop momenta generated by the product of trees in terms of the basis integrals [131–133]. The on-shell conditions $\delta(\ell^2)$ and $\delta((\ell + k_2 + k_3)^2)$ inside of dLIPS are then taken as a restriction to only keep basis elements in the reduction with at least those propagators.

All of the above can be generalized to higher loop orders via *generalized-unitarity cuts*. For a graph G in a particular theory, its generalized-unitarity cut is defined as

$$\text{Cut}_G = \sum_{\substack{\text{states} \\ \text{of } E(G)}} \prod_{v \in V(G)} \mathcal{A}_{\text{tree}}(v), \quad (3.8)$$

where $E(G)$ are the internal edges of G , all of which are taken on-shell, $V(G)$ are the vertices of G , and $\mathcal{A}_{\text{tree}}$ are the relevant tree amplitudes for the theory under consideration. For instance, we can write an iterated version of eq. (3.7) for gravitons as

$$\text{Diagram of a loop with 4 external legs and vertical dashed lines} = \sum_{\substack{\text{states of} \\ \{\ell_1, \ell_2, \ell_3, \ell_4\}}} \mathcal{M}_{\text{tree}}(1, 2, \ell_1, \ell_2) \mathcal{M}_{\text{tree}}(-\ell_1, -\ell_2, \ell_3, \ell_4) \mathcal{M}_{\text{tree}}(-\ell_3, -\ell_4, 3, 4). \quad (3.9)$$

Important to note is that it is often impossible to solve all of the cut conditions defining the on-shell loop momenta in terms of real-valued Lorentzian kinematics, so generalized unitarity methods are understood as complex-analytic tools for determining what rational

functions need to be integrated. The cuts themselves generally do not have support on the physical integration contour that produces the amplitude.

The sum over states in eq. (3.8) hides most of the complexity of cut construction. Since the focus of the current paper involves gravitational interactions, we restrict our attention to the particular case of only internal gravitons. In this situation, evaluating the state sum for each of the edges crossing the cut involves inserting a complete set of graviton states in D spacetime dimensions via

$$\sum_{\text{states}} \varepsilon_k^{\mu\nu} \varepsilon_k^{\alpha\beta} \equiv \mathcal{P}_k^{\mu\nu;\alpha\beta} = \frac{1}{2} \left(P_k^{\mu\alpha} P_k^{\nu\beta} + P_k^{\mu\beta} P_k^{\nu\alpha} - \frac{2}{D-2} P_k^{\mu\nu} P_k^{\alpha\beta} \right), \quad (3.10)$$

$$P_k^{\mu\nu} \equiv \eta^{\mu\nu} - \frac{k^\mu q^\nu + k^\nu q^\mu}{k \cdot q}, \quad (3.11)$$

in which q^μ is a null reference vector. The presence of q serves to make eq. (3.10) analogous to a gauge-agnostic graviton propagator (with $(k^2)^{-1}$ replaced with an implicit $\delta(k^2)$). In fact, gauge invariance of a cut with respect to the internal states manifests as q -independence of the cut. Explicitly removing the q dependence can be computationally intensive for complicated cuts. Ref. [134] provides an excellent discussion for effective ways of dealing with these types of D -dimensional state sums.

When a basis of integrals for a particular problem is known, generalized unitarity cuts can be used to identify the basis coefficients via

$$\frac{\text{Cut}_G}{|G|} = \sum_{\substack{\mathcal{I}_i \text{ has propagators} \\ \text{compatible with } E(G)}} c_i \mathcal{I}_i, \quad (3.12)$$

with $|G|$ the number of symmetries of the graph and where the sum is over integral basis elements which have at least the same propagators as $E(G)$. Integral basis identification and construction is often a highly non-trivial task involving many subtleties. As such, significant effort has been put into identifying particularly good choices of bases [99] and developing basis-agnostic methods [135, 136]. Luckily, we will see below that the tails have relatively simple and easy-to-identify integral bases. Even better, the matching between cuts and integral-basis coefficients is nearly a direct equality, modulo details about “non-planar” channels that will be discussed in situ.

4 The Tail Effect

The effective field theory approach has been extremely successful at using analogies with particle physics to improve the understanding of gravitational dynamics in the bound two-body problem. Further bringing modern amplitudes insights to bear has pushed the frontier for hyperbolic encounters in the scattering problem [33–40], and led to new developments in direct observable computations [137, 138]. However, in this work as well as in our preceding letter [47], we advocate applying both particle analogies and amplitudes methods *directly at the level of the composite binary to the gravitational radiation in the bound two-body problem*. The long-standing analogy between interactions of spin- $l/2$ elementary particles,

and of classical l -th multipole moments, and especially higher spin-induced multipoles S^l , [68, 139], applied in [69, 140], suggests that we can go further, and model even the multipole moments of the binary itself – in terms of fundamental particles interacting with gravity. By working with scattering amplitudes for the particle interactions, rather than Feynman rules, we will be able to construct the tail effective actions by combining gauge-invariant on-shell objects via the method of generalized unitarity. Doing so removes the need to care about graviton gauge choices, allows exploiting developments in amplitudes construction and integration, and more directly highlights the patterns that appear throughout the tails.

It is also worthwhile to discuss the link between the two-point and one-point EFT approaches to tails, which ties in significantly with a unitarity-based perspective. As discussed in section 2, the one-point approach deals with calculating the unpolarized cross-section of a graviton one-point function in the normal way, $\sum_h |\mathcal{A}_h|^2$. However, this process is almost exactly equivalent to computing *generalized unitarity cuts* (see section 3) in the two-point approach (up to shuffling of terms related to the regularization schemes). This is since the latter entails *inserting a complete set of graviton states between two on-shell amplitudes* as follows:

$$\int d\text{LIPS} \sum_h |\mathcal{A}_h|^2 = \text{diagram} \Rightarrow \text{diagram} , \quad (4.1)$$

where the **dashed colored lines** remain a shorthand for the on-shell state sum. With the far right-hand-side we are schematically conveying the diagrammatic expansion of \mathcal{A} and \mathcal{A}^\dagger using the diagram style of our two-point approach (as shall also be seen in our evaluations below), including scattering off of the potential modes sourced by the composite particle’s energy E . As usual the formal “all-orders” amplitudes are expanded so that the observable contains the desired order of contributions, including in this case the number of potential-mode interactions.

Thus, we can view our unitarity-based two-point formalism as alternatively being a method of directly calculating unpolarized graviton emission cross-sections without needing to construct the individual \mathcal{A} and \mathcal{A}^\dagger . See also a discussion on how this plays out at leading order in the recent Ref. [141]. Note that the exact perturbative equivalence between the two approaches depends on aligning various regularization conventions. For example, the two-point formalism applies dimensional regularization to all of the graviton loop integrations, while the standard dLIPS that appears in a cross-section computation normally uses a fixed integer dimension. Note that a full quantum-like “GR+matter” computation, like

that used in the PM approach, naturally aligns these conventions. Yet in the direct PN EFT approach this should be handled with care due to the splitting of graviton modes, as well as the treatment of matter components as classical sources.

4.1 Building Blocks

For the calculation of the tails, we will need three types of building blocks. First, we need to describe the interaction of a quadrupole with the gravitational field. The analogy between the interactions of classical l -th multipoles, in particular of higher-spin multipoles S^l , and of quantum spin $l/2$ particles, suggests that we model the “one-graviton source” associated to the quadrupole, as a 3-point amplitude of a spin-1 massive particle radiating a graviton. Extracting the quadrupole-coupling directly from a vector-graviton interaction is somewhat involved [139]. Thus we shall take a shortcut by using the double copy.

First, since the quadrupole is a symmetric traceless $SO(3)$ tensor, it can be represented as an outer product between two $SO(3)$ vectors

$$I_{ij} \equiv I_i I_j, \quad \delta^{ij} I_i I_j = 0. \quad (4.2)$$

The $SO(3)$ vectors can be covariantized so that in the rest frame of the binary we have $I^\mu = (0, I^i)$. Now we consider the fermion-to-spin identification of Ref. [139]. Applied to the fermion-vector 3-point amplitude, and interpreting the spin vector S_i as the generic $SO(3)$ vector I^μ , we find

$$\mathcal{M}_{fvf} \propto \bar{u}(k_1) \not{\epsilon}_3 u(k_2) \rightarrow \left[\frac{(k_2 \cdot \epsilon_3)}{2m} \bar{u}(k_1) u(k_2) - \frac{i}{m^2} \varepsilon_{\mu\nu\rho\sigma} \epsilon_3^\mu k_1^\nu k_2^\rho I^\sigma \right], \quad (4.3)$$

where u, ε are the spinors and vector polarization, respectively. The second term is proportional to $\text{tr}(\gamma_5 \not{\epsilon}_3 \not{k}_2 \not{k}_1 \not{I})$, and the I dependence of both terms, which is implicit here in the first term, has the same structure in the non-relativistic limit.

Thus, we shall focus on how the explicit trace term

$$\mathcal{M}_{fvf} \Big|_I \propto \text{tr}(\gamma_5 \not{\epsilon}_3 \not{k}_2 \not{k}_1 \not{I}), \quad (4.4)$$

eventually generates the quadrupole-graviton coupling tensor structure via the double copy, and fix the overall coupling constant later. We take the double copy of eq. (4.4) with itself to produce a vector-graviton 3-point amplitude, with the explicit identification of the quadrupole component already made

$$\mathcal{M}_{vgv} \propto \mathcal{M}_{fvf}^2 \propto [\text{tr}(\gamma_5 \not{\epsilon}_3 \not{k}_2 \not{k}_1 \not{I})]^2. \quad (4.5)$$

The square of the parity-odd trace produces a Gram determinant, which evaluates to

$$\mathcal{M}_{Ig} \propto \text{GramDet}(k_2, k_1, I, \varepsilon_g) = \tilde{\lambda} [(\varepsilon_g \cdot k_1)(I \cdot k_g) - (\varepsilon_g \cdot I)(k_1 \cdot k_g)]^2, \quad (4.6)$$

after applying momentum conservation and external state conditions, and absorbing constants into $\tilde{\lambda}$.

Evaluating this coupling in the rest-frame of particle 1 yields

$$\begin{aligned}\mathcal{M}_{Ig} &\rightarrow \tilde{\lambda} m_1^2 (I^i k_g^i \varepsilon_g^0 - I^i \varepsilon_g^i \omega_g)^2 \\ &= \lambda_I I^{ij} (\omega_g k_g^i \varepsilon_g^0 \varepsilon_g^j + \omega_g k_g^j \varepsilon_g^0 \varepsilon_g^i - k_g^i k_g^j \varepsilon_g^0 \varepsilon_g^0 - \omega_g^2 \varepsilon_g^i \varepsilon_g^j),\end{aligned}\quad (4.7)$$

where the coupling constant λ_I remains to be fixed. Up to alignment of coupling constants this exactly agrees with the one-graviton quadrupole operator used throughout EFT-based approaches (see Refs. [17, 26, 88, 139, 142] for foundational discussions of these types of operators). We will write here

$$\mathcal{M}_{Ig} \equiv \lambda_I J_I^{\mu\nu} \varepsilon_{\mu\nu} = I^{ij} \blacksquare^{\mu\nu} \varepsilon_{\mu\nu}, \quad (4.8)$$

when discussing the quadrupole coupling amplitude in contexts where the polarizations may be stripped off. Since we are only focused on the tails of the quadrupole in this work, we do not require higher-graviton quadrupole couplings, or higher-multipole couplings.

Second, in addition to the quadrupole coupling, the tails specifically involve interactions with the gravitational potential of the system. This type of coupling is well understood to be analogous with minimal scalar-graviton interactions [17, 139]. As such, we take the potential-mode graviton source to be

$$\mathcal{M}_{Eg} = \mathcal{M}_{sgs} = \frac{\lambda_E}{m_s^2} p_s^\mu p_s^\nu \varepsilon_{\mu\nu} = E \bullet^{\mu\nu} \varepsilon_{\mu\nu}, \quad (4.9)$$

which in the rest frame of the scalar evaluates to $\lambda_E \varepsilon_{00}$, in agreement with the EFT definition of the static source of potential modes, $E h^{00}$, after appropriate alignment of coupling constants.

Third, beyond the three-point amplitude (analogous to a one-point source) for the potential-mode coupling, we will also require four-point amplitudes to capture the possible contact terms (analogous to a two-point source) in a gauge-invariant manner. The obvious choice for the desired amplitude is the two-graviton two-scalar extension of eq. (4.9), which is computable as the double-copy of a two-scalar two-gluon amplitude using [IncreasingTrees](#) as

$$\begin{aligned}\mathcal{M}_{Eg^2} \stackrel{?}{=} \mathcal{M}_{sggs} &= \frac{\lambda_E}{m_s^2} \lambda_g \left((\varepsilon_2 \cdot k_1)(\varepsilon_3 \cdot k_{12}) - \frac{1}{2}(\varepsilon_2 \cdot \varepsilon_3)(k_1 \cdot k_2) \right) \left[\right. \\ &\quad \left((\varepsilon_2 \cdot k_1)(\varepsilon_3 \cdot k_{12}) - \frac{1}{2}(\varepsilon_2 \cdot \varepsilon_3)(k_1 \cdot k_2) \right) \left(\frac{1}{2(k_1 \cdot k_2)} + \frac{1}{2(k_2 \cdot k_3)} \right) \\ &\quad \left. + \left((\varepsilon_2 \cdot k_{13})(\varepsilon_3 \cdot k_1) - \frac{1}{2}(\varepsilon_2 \cdot \varepsilon_3)(k_1 \cdot k_3) \right) \frac{1}{2(k_2 \cdot k_3)} \right] + (2 \leftrightarrow 3),\end{aligned}\quad (4.10)$$

in which particles 1 and 4 are the scalars, and 2, 3 the gravitons, all particles have the same external momentum flow, and λ_g is the graviton self-coupling constant to be fixed later.

However, the amplitude as-is contains too much information: it encodes not only the graviton self-interactions and contact terms, but also propagation of an off-shell scalar particle via the $p_1 \cdot p_2$ and $p_1 \cdot p_3$ poles. Including the off-shell propagation is in direct

tension with wanting to interpret the scalar as a classical massive object. The tension can be resolved by appealing to the identification of the scalar with a black hole: we treat the scalar mass as the dominant scale in the problem, and expand the four-point amplitude in said limit. Doing so in the rest frame of massive particle leads to

$$\begin{aligned}
\mathcal{M}_{Eg^2} = \mathcal{M}_{sggs}(m_s \rightarrow \infty) &= \frac{\lambda_g \lambda_E}{\omega_2^2} \frac{\delta(\omega_2 - \omega_3)}{2(k_2 \cdot k_3)} \left[(k_2 \cdot k_3) \varepsilon_2^0 \varepsilon_3^0 + \omega_2 ((\varepsilon_3 \cdot k_2) \varepsilon_2^0 \right. \\
&\quad \left. - (\varepsilon_2 \cdot k_3) \varepsilon_3^0) - \omega_2^2 (\varepsilon_2 \cdot \varepsilon_3) \right]^2 + \mathcal{O}(m_s^{-1}) \\
&= E \bullet \begin{array}{c} \varepsilon_1^{\mu\nu} \\ \text{~~~~~} \\ \varepsilon_2^{\rho\sigma} \end{array}, \tag{4.11}
\end{aligned}$$

in which we have put back in an explicit $\delta(\omega_2 - \omega_3)$ on the leading-order term that results from evaluating the normally-implicit momentum conserving $\delta^4(\sum k)$ in the large-mass limit. Note that this definition is equivalent, up to external momentum flow conventions and frame choices, with the “heavy-mass” amplitudes of Ref. [143].

Finally, we will need amplitudes for graviton self-interactions. For the work at hand, we only require tree amplitudes,³ which are easily constructed using the `IncreasingTrees` package. The tree amplitudes built by the package are normalized by setting the coefficients of specific kinematic structures to 1 rather than against a particular choice of coupling, so a coupling factor of λ_g^{n-2} must be included on all of the graviton tree amplitudes.

Throughout the above discussion, we introduced coupling constants that should be matched with appropriate references for comparisons to be accurate. We choose to specifically match against the conventions of Refs. [26, 27], making our coupling constants:

$$\begin{aligned}
\lambda_I &= \sqrt{2\pi G_N}, \\
\lambda_E &= -E \sqrt{8\pi G_N}, \\
\lambda_g &= -\sqrt{32\pi G_N}. \tag{4.12}
\end{aligned}$$

Notably we will use the fixed-dimension standard definition for G_N , and will introduce a renormalization scale μ that accounts for the scale-dependence of working in dimensional regularization.

4.2 Radiation-Reaction

The quadrupole-sourced radiation reaction (no interaction with the background potential), and leading tail, have been studied extensively [13, 15, 24–29, 88, 89, 91, 144], so serve as verifications for our proposed methods. They are also simple enough that we can present the majority of intermediate steps in detail.

Beginning with radiation reaction, there is only one diagram topology that we need to consider in both the EFT/Feynman and generalized-unitarity perspectives, namely fig. 1.

³This follows from the general philosophy that “tree level is classical”. While not true when matter loops are involved, the heuristic does hold for massless force-carrier loops. Ref. [137] provides a thorough exploration of the topic via explicit \hbar counting.

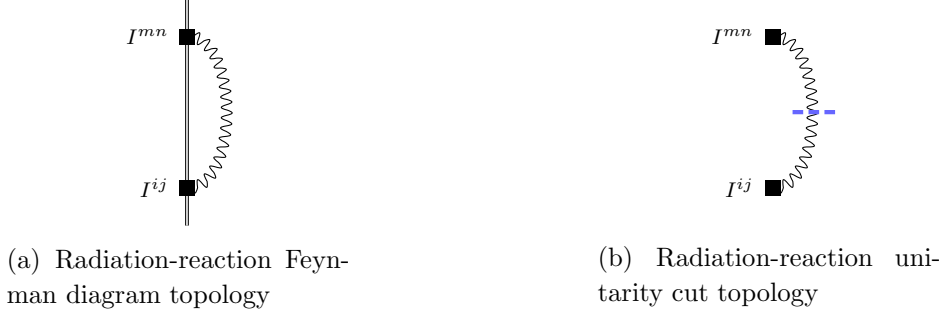


Figure 1: The quadrupole radiation-reaction diagrams.

This is rather straightforward to see. When we label the momentum flow of the gravitons in the Feynman diagram, fig. 1a, and impose momentum conservation (in this case non-existent), we find only a single momentum ℓ^μ and only one possible momentum invariant, $\ell^2 = \omega^2 - \ell_E^2$. Thus, the relevant integral family consists of

$$\int \frac{d^d \ell_E}{(2\pi)^d} \frac{\ell_E^{i_1} \dots \ell_E^{i_n}}{(-\ell_E^2 + \omega^2)^\lambda}, \quad \lambda \in \mathbb{Z}_+, n \geq 0. \quad (4.13)$$

In fact, symmetry and integral relations always allow us to write any integral of this type in terms of $\omega^n \delta^{i_1 \dots i_n}$ (see appendix A for a brief discussion of our systematic method for dealing with the tensor reductions appearing in the tails), and the single basis integral

$$F^{(1)}(1; \omega^2) = \int \frac{d^d \ell_E}{(2\pi)^d} \frac{1}{(-\ell_E^2 + \omega^2)} = -\frac{\Gamma(1 - d/2)(-\omega^2)^{d/2-1}}{(4\pi)^{d/2}}, \quad (4.14)$$

where d is the dimensional regularization dimension $d = 3 + \epsilon$ and ω has an imaginary part set by the $i0$ prescription for the propagator. In the Feynman prescription, the effective action would then be written as

$$S_{\text{RR}} = \int \frac{d\omega}{2\pi} c_{\text{RR}} F^{(1)}(1; \omega^2 + i0). \quad (4.15)$$

Working in the CTP prescription, we instead need to sum over advanced and retarded propagators. In turn, this means that the radiation reaction contribution to the CTP effective action *must* be expressible as

$$S_{\text{RR}} = \int \frac{d\omega}{2\pi} \left(c_{\text{RR}}^{-+} F^{(1)}(1; \omega_R^2) + c_{\text{RR}}^{+-} F^{(1)}(1; \omega_A^2) \right). \quad (4.16)$$

Our goal is now to determine c_{RR} using unitarity methods. It is also worth pointing out that the different $i0$ prescriptions change the way that the $\sqrt{-\omega^2}$ in eq. (4.14) (and later $\log(-\omega^2)$) will be analytically continued. The Feynman prescription tells us to do the continuation using a *fixed* imaginary part of ω^2 , while the advanced and retarded prescriptions tell us to treat the imaginary part as *depending on the sign of ω* .

Following the ideas discussed in section 3, c_{RR} should be directly related to the generalized unitarity cut of the diagram divided by the symmetry factor for the diagram. We

calculate the generalized unitarity cut, following eq. (3.8), as the product of two quadrupole amplitudes, eq. (4.8), summed over the $D = d+1$ -dimensional states of the internal graviton using eq. (3.10) to find

$$\begin{aligned}
\text{Cut}_{\text{RR}}^{ab} &= \sum_{\text{grav states}} \mathcal{M}_{I_a(-\omega)} \mathcal{M}_{I_b(\omega)} \\
&= \lambda_I^2 J_{I_a(-\omega)}^{\mu\nu} \mathcal{P}^{\mu\nu;\alpha\beta} J_{I_b(\omega)}^{\alpha\beta} \Big|_{\ell^2 = \omega^2 - \ell_E^2 = 0} \\
&= (2\pi G_N) \delta(\omega^2 - \ell_E^2) \left(J_{I_a(-\omega)}^{\mu\nu} J_{I_b(\omega)}^{\mu\nu} - \frac{J_{I_a(-\omega)}^{\mu\mu} J_{I_b(\omega)}^{\nu\nu}}{D-2} \right), \tag{4.17}
\end{aligned}$$

with CTP labels a, b . Inserting the definitions for $J^{\mu\nu}$ and performing tensor reductions following appendix A, we arrive at

$$\text{Cut}_{\text{RR}}^{ab} = (2\pi G_N) \kappa_{ab}(\omega) \omega^4 \frac{(d+1)(d-2)}{(d+2)(d-1)} \delta(\omega^2 - \ell_E^2). \tag{4.18}$$

We see that the cut only depends on the CTP labels through $\kappa^{ab}(\omega)$, and this turns out to be true for the rest of the calculations we will approach in this paper. As a result of this observation, we define the unindexed cut as

$$\text{Cut}_{\text{RR}}^{ab} \equiv \text{Cut}_{\text{RR}} \kappa_{ab}(\omega), \tag{4.19}$$

and slightly restructure the CTP effective action as

$$\begin{aligned}
S_{\text{RR}} &= \int \frac{d\omega}{2\pi} a_{\text{RR}} \left(\kappa_{-+}(\omega) F^{(1)}(1; \omega_R^2) + \kappa_{+-}(\omega) F^{(1)}(1; \omega_A^2) \right) \\
&\equiv \int \frac{d\omega}{2\pi} a_{\text{RR}} F_{\text{CTP}}^{(1)}(1; \omega^2). \tag{4.20}
\end{aligned}$$

This makes it clear that while a fully detailed treatment would involve separately matching coefficients between the different CTP branches, the net result of the matching in this case will be the same as if we had ignored the $i0$ prescription which only contributes through the integration contour of the basis integrals. This continues to occur for all of the higher-order tails considered below as well.

We proceed with reconstructing a_{RR} by matching the cut against the basis integral. Because the cut is already independent of the loop momentum, we do not have any reduction to perform. Thus the matching process is very simple

$$\text{Cut}_{\text{RR}} = (2\pi G_N) \omega^4 \frac{(d+1)(d-2)}{(d+2)(d-1)} \delta(\omega^2 - \ell_E^2) = |G_{\text{RR}}| a_{\text{RR}} \delta(\omega^2 - \ell_E^2). \tag{4.21}$$

We now need to determine the symmetry factor $|G_{\text{RR}}|$. The purpose of dividing by the symmetry factor is to compensate for possible over-counting of redundant information by the cut. Since our implementation of CTP sums over the advanced and retarded branches, we need to make sure that the cut is not double-counting contributions across branches. The simplest way to do so is to count the up/down reflection (in our drawing convention) as

a symmetry of the cut. Thus, in the current case we have $|G_{\text{RR}}| = 2$. Many of the diagrams for the higher-order tails also include this reflection as part of the symmetry factor. Putting everything together leads to our CTP effective action for radiation reaction

$$S_{\text{RR}} = \frac{(2\pi G_N)(d+1)(d-2)}{2(d+2)(d-1)} \int \frac{d\omega}{2\pi} \omega^4 F_{\text{CTP}}^{(1)}(1; \omega^2). \quad (4.22)$$

Inserting the master integral definition from eq. (4.14), expanding in $d = 3 + \epsilon^4$, and performing the CTP sum, we arrive at

$$S_{\text{RR}} = -i \frac{G_N}{5} \int \frac{d\omega}{2\pi} \omega^5 \kappa_{-+}(\omega) \left[1 - \frac{\epsilon}{2} \left(i\pi \operatorname{sgn} \omega + \left[\frac{9}{10} - \log \left(\frac{\omega^2 e^{\gamma_E}}{\mu^2 \pi} \right) \right] \right) + \mathcal{O}(\epsilon^2) \right], \quad (4.23)$$

in which we have introduced the standard renormalization scale to the logarithm, and have retained the $\mathcal{O}(\epsilon^1)$ piece for later use in counterterm analysis. Note also the appearance of the $i\pi \operatorname{sgn} \omega$ term, which is a result of using the modified $i0$ prescription. The standard QFT Feynman prescription would produce a definite sign rather than the $\operatorname{sgn} \omega$.

4.3 Tail

We are now ready to approach the leading tail calculation. The broad strokes are similar to the radiation reaction, with just a few new pieces necessary for the higher tails. From now on, we drop the explicit E label on the loop momenta as we will always be working with integrated Euclidean loop momenta and an explicit frequency as the scale.

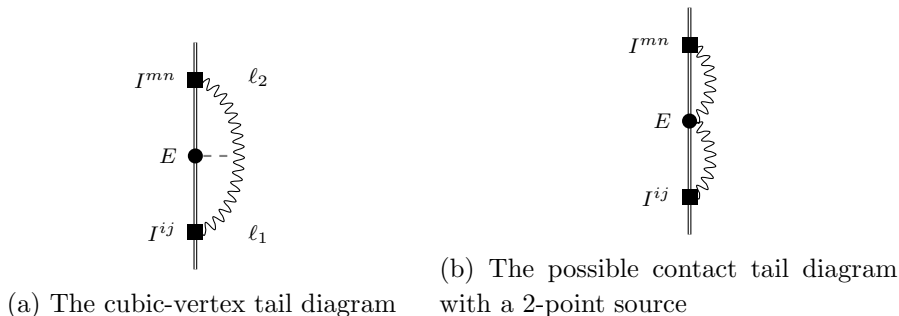


Figure 2: The possible Feynman diagrams needed to evaluate the leading tail contribution.

The first important development is that there is more than one Feynman diagram, with a single energy coupling (analogous to the so-called “self-energy” graphs), that contributes to the process (depending on gauge choices), shown in fig. 2. Therefore we should take some care with defining our basis of momentum invariants and integral family. A maximally convenient basis of momentum invariants to use is one which contains all possible inverse propagators of the diagrams under consideration. For the tail diagrams, we can use the labelings of ℓ_1 and ℓ_2 as shown in fig. 2a to define the inverse propagator basis

$$Q_1 = \omega^2 - \ell_1^2, \quad Q_2 = \omega^2 - \ell_2^2, \quad Q_3 = -(\ell_1 + \ell_2)^2, \quad (4.24)$$

⁴Note that our choice of d differs from the standard analytic continuation of $d - d_z = -2\epsilon$. This choice will of course drop out of the final observables.

with signs set by a mostly-minus metric to best align with the standard integration convention for propagator signs, see appendix B.1 for more details, and where we have now made the fact that the ℓ_i are the Euclidean spatial part of the momenta implicit. Important to note is that Q_3 is chosen as a purely spatial momentum: it is the “potential-mode” propagator expected from the interaction of the quadrupole with the static background potential. From this basis, it is obvious that the integral family we need to consider is

$$F^{(2)}(\lambda_1, \lambda_2, \lambda_3) = \int \prod_{i=1}^2 \left(\frac{d^d \ell_i}{(2\pi)^d} \right) Q_1^{-\lambda_1} Q_2^{-\lambda_2} Q_3^{-\lambda_3}, \quad (4.25)$$

as it will cover any possible contributions from both diagram topologies. Analyzing the integral family, we again find a single basis integral, $F^{(2)}(1, 1, 0)$, implying that the effective action can be written as

$$\begin{aligned} S_T &= \int \frac{d\omega}{2\pi} \left(c_T^- F^{(2)}(1, 1, 0; \omega_R^2) + c_T^+ F^{(2)}(1, 1, 0; \omega_A^2) \right) \\ &\equiv \int \frac{d\omega}{2\pi} a_T F_{\text{CTP}}^{(2)}(1, 1, 0). \end{aligned} \quad (4.26)$$

There are two interesting observations about the integral basis. First, the basis integral actually factorizes! Q_1 and Q_2 depend separately on the two loop momenta so we have

$$F^{(2)}(1, 1, 0) = \left(\int \frac{d^d \ell_1}{(2\pi)^d} \frac{1}{Q_1} \right) \left(\int \frac{d^d \ell_2}{(2\pi)^d} \frac{1}{Q_2} \right) = F^{(1)}(1; \omega^2)^2. \quad (4.27)$$

Since $F^{(1)}(1; \omega^2)$ is finite in dimensional regularization, so is $F^{(2)}(1, 1, 0)$. Second, we have the important integral relation

$$F^{(2)}(1, 1, 1) = -\frac{(d-2)}{2(d-3)\omega^2} F^{(2)}(1, 1, 0). \quad (4.28)$$

This relation highlights that the only source of divergences in the tail comes from terms in which all three propagators are present.



(a) The unitarity cut diagram needed to evaluate the leading tail contribution (b) The unitarity cut used to check the pole of the basis cut.

Figure 3: The unitarity cut diagrams used for analysis of the tail.

Now that we have identified the basis integral, we set out to evaluate the corresponding cut. From the basis integral, we know that the needed cut must contain two radiation mode propagators. Within the tail framework, there is only one possible configuration of tree amplitudes with two radiation propagators: the quadrupole-mass-quadrupole contraction

with a two-point mass amplitude, as shown in fig. 3a. Assembling the cut as the product of tree amplitudes from eqs. (4.8) and (4.11) and inserting the sum over graviton states, we have

$$\begin{aligned} \text{Cut}_{\text{T}}^{ab} &= \sum_{\text{states}} \mathcal{M}_{I(-\omega)} \mathcal{M}_{Eg^2} \mathcal{M}_{I(\omega)} \Big|_{Q_1=0, Q_2=0} \\ &= \lambda_I^2 J_{I_a(-\omega)}^{\mu\nu} P^{\mu\nu;\alpha\beta} \mathcal{M}_{Eg^2}^{\alpha\beta;\gamma\sigma} P^{\gamma\sigma;\rho\tau} J_{I_b(\omega)}^{\rho\tau} \delta(Q_1) \delta(Q_2). \end{aligned} \quad (4.29)$$

Evaluating the contractions and performing the tensor reduction to $\kappa_{ab}(\omega)$ (but not employing IBP reductions yet), we arrive at

$$\begin{aligned} \text{Cut}_{\text{T}} &= \frac{4\pi^2 G_N^2 E(d-2)}{(d-1)^3(d+2)\omega^2} \delta(Q_1) \delta(Q_2) \left((d-2)Q_3^3 + 8(d-2)Q_3^2\omega^2 + 4(d^2+4d-9)Q_3\omega^4 \right. \\ &\quad \left. + 16(d^2-1)\omega^6 + \frac{8(d^2-1)(d+1)\omega^8}{Q_3} \right). \end{aligned} \quad (4.30)$$

Importantly, if we had used the full two-scalar two-graviton amplitude, eq. (4.10), instead of eq. (4.11), \mathcal{M}_{Eg^2} , then the ‘‘virtual black hole’’ poles would have entered the cut carrying dependence on the reference vector q from the physical state projector, eq. (3.10). The dependence on q drops exactly for the leading-order term in the large- m_s expansion. We have written the cut as a Laurent series in the uncut momentum invariant Q_3 to manifest the factorization property. This allows us to verify the Q_3^{-1} part of the cut by evaluating a different cut, the one shown in fig. 3b. This new cut is built from the one-point mass term, eq. (4.9), as well as a three-point all-graviton amplitude. Evaluating it, we find

$$\begin{aligned} \text{Cut}_{\text{fig. 3b}} &= \lambda_I^2 \left(J_{I_a(-\omega)}^{\mu_1\nu_1} P^{\mu_1\nu_1;\mu_2\nu_2} \right) \mathcal{M}_{ggg}^{\mu_2\nu_2;\alpha_2\beta_2;\rho_2\tau_2} \\ &\quad \times \left(P^{\alpha_2\beta_2;\alpha_1\beta_1} \mathcal{M}_{sgs}^{\alpha_1\beta_1} \right) \left(P^{\rho_2\tau_2;\rho_1\tau_1} J_{I_b(\omega)}^{\rho_1\tau_1} \right) \delta(Q_1) \delta(Q_2) \delta(Q_3) \\ &= \frac{32\pi^2 G_N^2 E(d-2)(d^2-1)(d+1)}{(d-1)^3(d+2)} \omega^6 \delta(Q_1) \delta(Q_2) \delta(Q_3), \end{aligned} \quad (4.31)$$

in exact agreement with the Q_3 residue of eq. (4.30). The polynomial-in- Q terms are known in the language of generalized unitarity as ‘‘contact’’ terms because they correspond to diagrams in which some propagators have been collapsed into a contact-like interaction.

The basis cut in eq. (4.30) is still a function of the loop momentum via Q_3 . Thus in order to match it with a_{T} , we need to reduce it using integration-by-parts relations [123–125]. Since there is only one basis integral, we do not need to worry about the support of the δ s. We use FIRE6 [145] to automate the reduction process, after which we find

$$\overline{\text{Cut}}_{\text{T}} = -16G_N^2 \pi^2 \omega^4 \frac{(d-2)(12-2d+5d^2-4d^3+d^4)}{(d-3)(d-1)^2 d(d+2)} \delta(Q_1) \delta(Q_2). \quad (4.32)$$

For later use, we name the polynomial of d occurring in the numerator as

$$\mathcal{P}_4 = 12 - 2d + 5d^2 - 4d^3 + d^4. \quad (4.33)$$

Constructing the coefficient in the effective action, eq. (4.26), now only requires normalizing by the symmetry factor of the graph, $|G_{\text{T}}| = 2$. Thus we have

$$S_{\text{T}} = -8G_N^2 \pi^2 \frac{(d-2)(12-2d+5d^2-4d^3+d^4)}{(d-3)(d-1)^2 d(d+2)} \int \frac{d\omega}{2\pi} \omega^4 F_{\text{CTP}}^{(2)}(1, 1, 0). \quad (4.34)$$

The basis integral is straightforward to evaluate using eq. (4.27). Even though the basis integral is finite, the coefficient now contains an explicit pole in $d_{\text{crit}} = 3$. Thus we need to expand the entire action using the dimension regularization $d = 3 + \epsilon$, yielding

$$\begin{aligned} S_{\text{T}} = \frac{2}{5} G_N^2 E \int \frac{d\omega}{2\pi} \omega^6 \kappa_{-+}(\omega) & \left\{ \frac{1}{\epsilon} + \left(\log \left(\frac{\omega^2 e^{\gamma_E}}{\mu^2 \pi} \right) - \frac{41}{30} - i\pi \text{sgn}(\omega) \right) \right. \\ & + \epsilon \left[-i\pi \text{sgn}(\omega) \left(\log \left(\frac{\omega^2 e^{\gamma_E}}{\mu^2 \pi} \right) - \frac{41}{30} \right) \right. \\ & \left. \left. + \log \left(\frac{\omega^2 e^{\gamma_E}}{\mu^2 \pi} \right) \left(\frac{1}{2} \log \left(\frac{\omega^2 e^{\gamma_E}}{\mu^2 \pi} \right) - \frac{41}{30} \right) - \frac{9}{4} \zeta_2 + \frac{3667}{1800} \right] + \mathcal{O}(\epsilon^2) \right\}. \end{aligned} \quad (4.35)$$

As already noted in [47] this effective action agrees with the one derived by Galley et al in Ref. [27] up to the overall sign.

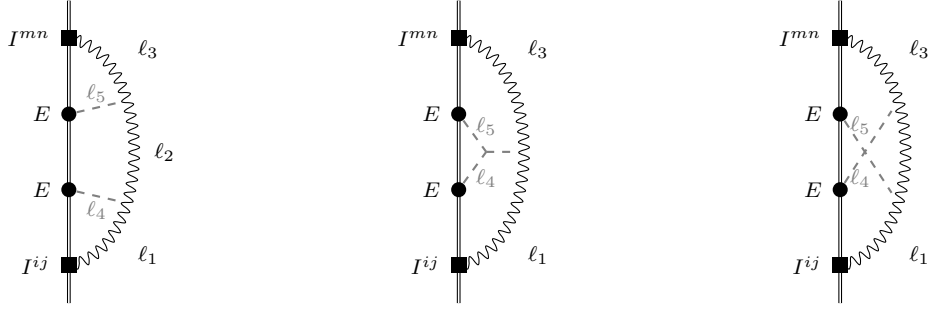
5 Higher-Order Tails

With the building blocks at our disposal, and well-known leading tail effects demonstrated in our methodology, we are ready to address higher-order tails. In this section we discuss the computation of the CTP effective action contributions for T^2 through T^4 . In our preceding letter [47] the T^2 and T^3 effective actions have been computed for the first time, which we present here in detail. We additionally provide in this paper the first newly-computed T^4 effective action.

5.1 Tail-of-Tail

We now proceed to the tail-of-tail calculation. As in the previous cases, our first task is to identify our basis of momentum invariants and the associated integral family. With two energy couplings, we will have 3 free loop momenta from which to build momentum invariants. A quick counting shows us that whatever basis of invariants we choose needs to cover $3 \ell_i^2$ plus $\binom{3}{2} = 3$ independent choices of $\ell_i \cdot \ell_j$. In line with what we did for the tail, it is useful to analyze the cubic tail-of-tail diagrams, shown in fig. 4, to cover as much of the momentum basis as possible using inverse propagators. All diagrams have 5 propagators, but only 4 can be chosen in common between fig. 4a and fig. 4b: $\omega^2 - \ell_1^2$, $\omega^2 - \ell_3^2$, $-\ell_4^2$, $-\ell_5^2$ are propagators in both. However, this means that the unique propagators in each diagram, $\omega^2 - \ell_2^2$ in fig. 4a and $-(\ell_1 + \ell_3)^2$ in fig. 4b can make up the fifth and sixth needed invariants. We make the following particular labeling choice:

$$\begin{aligned} Q_1 &= \omega^2 - \ell_1^2, & Q_2 &= \omega^2 - \ell_3^2, \\ Q_3 &= -\ell_4^2, & Q_4 &= -\ell_5^2 = -(\ell_1 + \ell_4 + \ell_3)^2, \\ Q_5 &= \omega^2 - \ell_2^2 = \omega^2 - (\ell_1 + \ell_4)^2, & Q_6 &= -(\ell_1 + \ell_3)^2. \end{aligned} \quad (5.1)$$



(a) The cubic tail-of-tail diagram with three radiation propagators and two potential propagators. (b) The cubic tail-of-tail diagram with two radiation propagators and three potential propagators. (c) The cubic tail-of-tail diagram with non-planar propagators.

Figure 4: The tail-of-tail diagrams with cubic vertices that are used to select an advantageous basis of momentum invariants.

At this point, it is also worth pointing out that there is an additional “non-planar” propagator $\omega^2 - (\ell_1 + \ell_5)^2 = Q_1 + Q_2 + Q_3 + Q_4 - Q_5 - Q_6$ that could appear through a diagram like fig. 4c, which appears to spoil the ability to define a single integral family to cover all possible propagator structures. In particular it will show up later through the u -channel pole of a four-graviton amplitude. However, since we are working to leading order in G_N , we expect the energy couplings to be time-independent and thus indistinguishable. This means that we can “uncross” the legs in fig. 4c (and similar diagrams) which results in fig. 4a (or similar) *except with* $\ell_4 \leftrightarrow \ell_5$, allowing us to rewrite any integrals that appear with a $\omega^2 - (\ell_1 + \ell_5)^2$ pole back in terms of the propagator basis using the relabeling $Q_5 \rightarrow Q_1 + Q_2 + Q_3 + Q_4 - Q_5 - Q_6$.

With the non-planar consideration dealt with, we have successfully identified all propagators that can appear and used them to span the set of momentum invariants. Thus, we capture all possible contributions coming from fig. 4 or their contact diagrams using the single integral family

$$F^{(3)}(\lambda_1, \lambda_2, \lambda_3, \lambda_4, \lambda_5, \lambda_6) = \int \left(\frac{d^d \ell}{(2\pi)^d} \right)^3 \frac{1}{Q_1^{\lambda_1} Q_2^{\lambda_2} Q_3^{\lambda_3} Q_4^{\lambda_4} Q_5^{\lambda_5} Q_6^{\lambda_6}}, \quad (5.2)$$

with integer values of λ_i . This integral family can be reduced in terms of two relevant basis integrals⁵

$$\mathcal{I}^{(3)} = \{F^{(3)}(1, 1, 0, 0, 1, 0), F^{(3)}(1, 1, 1, 1, 0, 0)\}, \quad (5.3)$$

with topologies corresponding to the unitarity cut diagrams shown in fig. 5. Thus the effective action for the tail-of-tail will be

$$S_{\text{TT}} = \int \frac{d\omega}{2\pi} \left[a_{\text{TT},1} F_{\text{CTP}}^{(3)}(1, 1, 0, 0, 1, 0) + a_{\text{TT},2} F_{\text{CTP}}^{(3)}(1, 1, 1, 1, 0, 0) \right]. \quad (5.4)$$

⁵The basis technically has additional integrals in it, for instance $F^{(3)}(1, 0, 0, 1, 1, 1)$, due to a rotational symmetry of the graphical representation of the family. This rotational symmetry is broken in the actual computation by the identification of which radiation propagator is sourced from which quadrupole.

We now proceed to evaluate the cuts in fig. 5 to determine $a_{\text{TT},1}$ and $a_{\text{TT},2}$.



(a) The double-contact TT diagram (b) The bulk contact TT diagram

Figure 5: The unitarity cut diagrams needed to evaluate the tail-of-tail.

The process for evaluating the first cut, fig. 5a, proceeds almost identically to evaluating the tail cut. We have

$$\begin{aligned} \text{Cut}_{\text{fig. 5a}} &= \lambda_I^2 \delta(Q_1) \delta(Q_2) \delta(Q_5) J_{I(-\omega)}^{\mu_1 \nu_1} P^{\mu_1 \nu_1; \mu_2 \nu_2} \mathcal{M}_{Eg^2,1}^{\mu_2 \nu_2; \mu_3 \nu_3} \\ &\quad \times P^{\mu_3 \nu_3; \mu_4 \nu_4} \mathcal{M}_{Eg^2,2}^{\mu_4 \nu_4; \mu_5 \nu_5} P^{\mu_5 \nu_5; \mu_6 \nu_6} J_{I(\omega)}^{\mu_6 \nu_6}, \end{aligned} \quad (5.5)$$

where we have added subscripts to the \mathcal{M}_{Eg^2} amplitudes to distinguish the two momentum labelings. Inserting the relevant definitions and evaluating all of the index contractions results in an expression that is hundreds of terms long, but has the general structure

$$\begin{aligned} \text{Cut}_{\text{fig. 5a}} &= (512G_N^3 E^2 \pi^3) \delta(Q_1) \delta(Q_2) \delta(Q_5) \left(\frac{1}{Q_3 Q_4} g_1(Q_6, \omega, d) + \frac{1}{Q_3} g_2(Q_4, Q_6, \omega, d) \right. \\ &\quad \left. + \frac{1}{Q_4} g_3(Q_3, Q_6, \omega, d) + g_4(Q_3, Q_4, Q_6, \omega, d) \right), \end{aligned} \quad (5.6)$$

where each of the g_i are polynomials in the Q s, but rational in d and ω . This specific form of the cut highlights the available factorization channels that can be cross-checked: g_2 and g_3 are partial contacts that can be checked by calculating the relevant cuts; g_1 is a channel that *overlaps* with fig. 5b and thus serves both as a check and as demonstration for why symmetry factors are necessary in the cut matching process, which we will show after constructing the other cut.

To constrain the integral basis coefficients using the cut, we must reduce it to the basis. As before, we do so by treating the $\delta(Q_i)$ s as propagators and reducing using standard methods, but since we have more than one basis element, the $\delta(Q_i)$ s instruct us to only keep the parts of the reduction which have at least Q_1 , Q_2 , and Q_5 as propagators. In particular, the g_2 , g_3 , and g_4 terms produce only the needed contributions, but the reduction of the g_1 term will produce both basis elements. We only keep the one involving $F^{(3)}(1, 1, 0, 0, 1, 0)$. Performing the reduction in this manner, we arrive at

$$\begin{aligned} \overline{\text{Cut}}_{\text{fig. 5a}} &= (512G_N^3 E^2 \pi^3) \frac{(d-2)(12-2d+5d^2-4d^3+d^4)^2 \omega^4}{4(d-3)^2(d-1)^3 d^2(d+1)(d+2)} \delta(Q_1) \delta(Q_2) \delta(Q_5) \\ &= (512G_N^3 E^2 \pi^3) \frac{(d-2) \mathcal{P}_4^2 \omega^4}{4(d-3)^2(d-1)^3 d^2(d+1)(d+2)} \delta(Q_1) \delta(Q_2) \delta(Q_5). \end{aligned} \quad (5.7)$$

We now turn our attention to the second cut, fig. 5b, which is constructed as

$$\text{Cut}_{\text{fig. 5b}} = \lambda_I^2 (J_{I(-\omega)} P)^{\mu_1 \nu_1} (\mathcal{M}_{sgs,1} P)^{\mu_2 \nu_2} \mathcal{M}_4^{\mu_1 \nu_1 \dots \mu_4 \nu_4} (P \mathcal{M}_{sgs,2})^{\mu_3 \nu_3} (P J_{I(\omega)})^{\mu_4 \nu_4}. \quad (5.8)$$

This cut is also almost one hundred terms long, but has the schematic form

$$\begin{aligned} \text{Cut}_{\text{fig. 5b}} = (512 G_N^3 E^2 \pi^3) & \delta(Q_1) \delta(Q_2) \delta(Q_3) \delta(Q_4) \left(\frac{1}{Q_5} h_1(Q_6, \omega, d) + \frac{1}{Q_6} h_2(Q_5, \omega, d) \right. \\ & \left. + \frac{1}{Q_5 + Q_6} h_3(Q_5 - Q_6, \omega, d) + h_4(Q_5, Q_6, \omega, d) \right), \quad (5.9) \end{aligned}$$

with the h_i having similar properties as the g_i above. The arrangement is again chosen to manifest pole structures and factorization: h_2 contains all contributions with the pole structures of fig. 4b, h_1 all those with the poles of fig. 4a, h_3 from fig. 4c, and h_4 the contact contribution.

From here we can delve into the overlapping channels to highlight the internal consistency checks and the need for relative symmetry factors. The objects of interest for the discussion are the overlapping channels from eq. (5.6) and eq. (5.9)

$$\begin{aligned} g_1(Q_6, \omega, d) &= h_1(Q_6, \omega, d) = -h_3(Q_5 - Q_6, \omega, d) \\ &= \frac{1}{8(d-1)^3(d+2)} \left[(-2+d)^2 Q_6^4 + 4(-2+d)^2 Q_6^3 \omega^2 \right. \\ &+ 4(d-1)(-9+d+d^2) Q_6^2 \omega^4 + 8(-2+d)(-1+d)(1+d) Q_6 \omega^6 \\ &\left. + 8(-2+d)(-1+d)^2(1+d) \omega^8 \right]. \quad (5.10) \end{aligned}$$

We immediately see that the overlapping channels agree: when we evaluate the $Q_3 = Q_4 = 0$ residue of eq. (5.6), essentially picking out the g_1 contribution, we get exactly the same expression as when evaluating the $Q_5 = 0$ residue of eq. (5.9). However, when we “uncross” the $Q_5 + Q_6$ pole using $Q_5 \rightarrow -Q_5 - Q_6$ (the consequence of the $\ell_4 \leftrightarrow \ell_5$ relabeling, with the help of the on-shell conditions), the cut becomes

$$\begin{aligned} \text{Cut}_{\text{fig. 5b}} = (512 G_N^3 E^2 \pi^3) & \delta(Q_1) \delta(Q_2) \delta(Q_3) \delta(Q_4) \left(\frac{1}{Q_5} 2h_1(Q_6, \omega, d) + \frac{1}{Q_6} h_2(Q_5, \omega, d) \right. \\ & \left. + h_4(Q_5, Q_6, \omega, d) \right). \quad (5.11) \end{aligned}$$

Through the $Q_5^{-1} 2h_1(Q_6, \omega, d)$ term, we see that $\text{Cut}_{\text{fig. 5b}}$ is actually double-counting its contribution with respect to $\text{Cut}_{\text{fig. 5a}}$. This misalignment is exactly what is compensated for by the $|G|$ normalization of cut matching, eq. (3.12). In the current case, the diagram of fig. 5b has an extra symmetry of swapping the energy sources (or $\ell_4 \leftrightarrow \ell_5$ as we actually use it) that fig. 5a does not have.

After the uncrossing, it is now also straightforward to reduce the cut. Again we only keep the reductions with propagators aligning with the $\delta(Q_i)$, namely those producing $F^{(3)}(1, 1, 1, 1, 0, 0)$. Doing so yields

$$\begin{aligned} \overline{\text{Cut}}_{\text{fig. 5b}} &= (512 G_N^3 E^2 \pi^3) \omega^6 \delta(Q_1) \delta(Q_2) \delta(Q_3) \delta(Q_4) \quad (5.12) \\ &\times \frac{(2d-3)(960 - 1696d + 424d^2 - 476d^3 + 330d^4 - 39d^5 + 53d^6 - 45d^7 + 9d^8)}{3(d-3)(d-1)^3 d(d+1)(d+2)(3d-4)(3d-2)}. \end{aligned}$$

We similarly name the d polynomial in the numerator

$$\mathcal{P}_8 = 960 - 1696d + 424d^2 - 476d^3 + 330d^4 - 39d^5 + 53d^6 - 45d^7 + 9d^8. \quad (5.13)$$

With both cuts in hand, we can now construct the effective action. The cuts are again in one-to-one correspondence with the coefficients,

$$a_{TT,1} \delta(Q_1)\delta(Q_2)\delta(Q_5) = \frac{\overline{\text{Cut}}_{\text{fig. 5a}}}{|G_{\text{fig. 5a}}|} = \frac{\overline{\text{Cut}}_{\text{fig. 5a}}}{2}, \quad (5.14a)$$

$$a_{TT,2} \delta(Q_1)\delta(Q_2)\delta(Q_4)\delta(Q_5) = \frac{\overline{\text{Cut}}_{\text{fig. 5b}}}{|G_{\text{fig. 5b}}|} = \frac{\overline{\text{Cut}}_{\text{fig. 5b}}}{4}. \quad (5.14b)$$

The integrals themselves are straightforward to evaluate. $F^{(3)}(1, 1, 0, 0, 1, 0)$ is just the cube of a one-propagator integral, while $F^{(3)}(1, 1, 1, 1, 0, 0)$ is evaluable via bubble iteration. More details on the evaluations are provided in appendix B.1. We thus have all of the information required to construct the tail-of-tail effective action via eq. (5.4). Expanding in $d = 3 + \epsilon$ and performing the CTP sum yields

$$\begin{aligned} S_{\text{TT}} = \frac{214}{525} G_N^3 E^2 \int \frac{d\omega}{2\pi} \omega^7 \kappa_{-+}(\omega) & \left\{ \frac{i}{\epsilon} + \left[\frac{3}{2} i \log \left(\frac{\omega^2 e^{\gamma_E}}{\mu^2 \pi} \right) + \frac{3\pi \operatorname{sgn}(\omega)}{2} - \frac{420}{107} i \zeta_2 - \frac{675359}{89880} i \right] \right. \\ & + \epsilon \left[\pi \operatorname{sgn}(\omega) \left(\frac{9}{4} \log \left(\frac{\omega^2 e^{\gamma_E}}{\mu^2 \pi} \right) - \frac{(352800 \zeta_2 + 675359)}{59920} \right) \right. \\ & + i \log \left(\frac{\omega^2 e^{\gamma_E}}{\mu^2 \pi} \right) \left(\frac{9}{8} \log \left(\frac{\omega^2 e^{\gamma_E}}{\mu^2 \pi} \right) - \frac{(352800 \zeta_2 + 675359)}{59920} \right) \\ & \left. \left. + \frac{4569}{856} i \zeta_2 - \frac{1050}{107} i \zeta_3 + \frac{1259125247}{37749600} i \right] + \mathcal{O}(\epsilon^2) \right\}, \quad (5.15) \end{aligned}$$

with ζ_n the Riemann zeta values: $\zeta_2 = \frac{\pi^2}{6}$, $\zeta_3 = 1.20206 \dots$, $\zeta_4 = \frac{\pi^4}{90}$, etc. This result, first reported in Ref. [47], is the first time the tail-of-tail effective action as been computed.

5.2 Tail-of-Tail-of-Tail

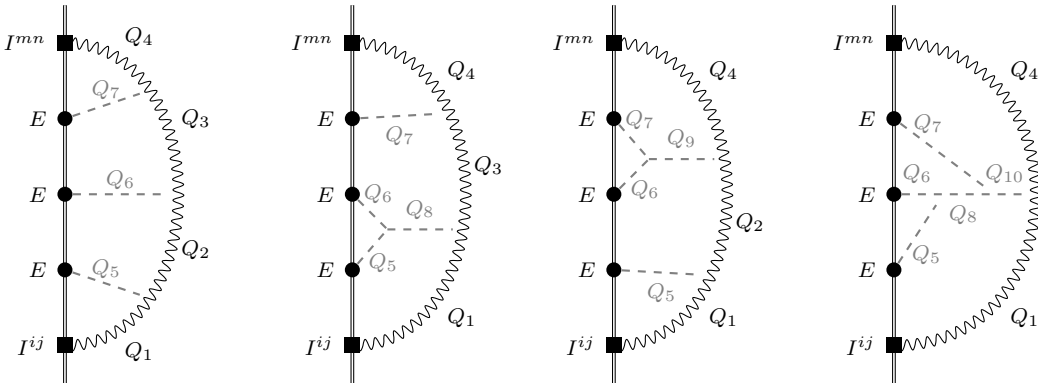


Figure 6: The cubic TTT diagrams that are used to select a basis of momentum invariants

There are few new features to the process of calculating TTT. It is primarily a proliferation of all features. First, we have a momentum-invariants basis with $\binom{4}{2} + 4 = 10$ elements that we need to choose. We use the cubic diagrams shown in fig. 6 to define the set of propagators we select as a basis. There are significantly more “uncrossing” relabelings that can be used to return non-planar pole structures back to the basis, all of which we will need to employ when expanding higher-point graviton amplitudes. Thus we still only need a single integral family, given by

$$F^{(4)}(\lambda_1, \dots, \lambda_{10}) = \int \left(\frac{d^d \ell}{(2\pi)^d} \right)^4 \frac{1}{\prod_{i=1}^{10} Q_i^{\lambda_i}}. \quad (5.16)$$

The relevant basis integrals are

$$\mathcal{I}^{(4)} = \{F^{(4)}(1, 1, 1, 1, 0, 0, 0, 0, 0, 0), F^{(4)}(1, 0, 0, 1, 1, 1, 1, 0, 0, 0), \\ F^{(4)}(1, 0, 1, 1, 1, 1, 0, 0, 0, 0), F^{(4)}(1, 1, 0, 1, 0, 1, 1, 0, 0, 0)\}, \quad (5.17)$$

which correspond to the topologies in fig. 7. The first, third, and fourth basis integrals are all factorizable, while the third is evaluable via bubble iteration. Notably, the last two integrals are actually equal: the integrals both factorize in exactly the same way so it does not matter whether the one-propagator piece occurs first or last in the evaluation. Thus, at the level of the CTP sum, the $-+$ orientation of one diagram exactly matches the $+ -$ of the other. We could use this symmetry to remove one of the two integrals and corresponding cut from the basis, at which point it would *no longer carry the reflection symmetry factor*. Instead we keep both contributions and the reflection symmetry factor will remove the over-count of keeping both. This allows an explicit verification that both diagrams have identical contributions so either approach would produce the same result.

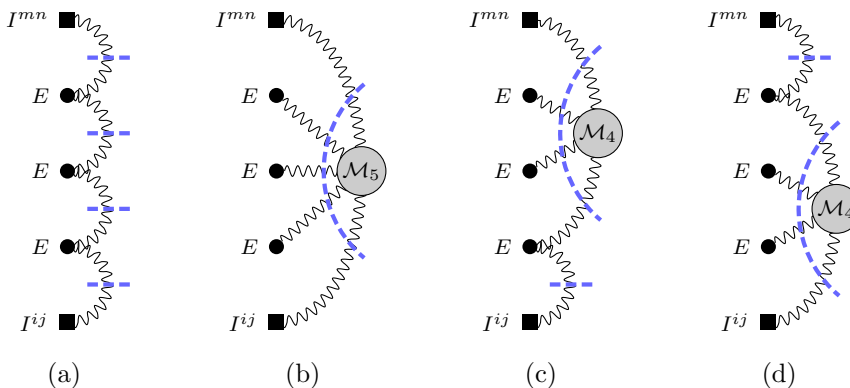


Figure 7: The TTT unitarity cuts.

The cuts are still one-to-one with the basis coefficients, so we simply need the symmetry factors of each cut, which come from the number of equivalent rearrangements of the E -connected lines along with the reflection symmetry

$$|G_{\text{fig. 7a}}| = 2, \quad |G_{\text{fig. 7b}}| = 2 \times 3! = 12, \quad |G_{\text{fig. 7c}}| = |G_{\text{fig. 7d}}| = 2 \times 2! = 4, \quad (5.18)$$

along with each of the reduced cuts. The corresponding cuts are all thousands of terms long prior to reduction, but after reduction each one produces a basis coefficient that is a relatively simple rational function of d and ω :

$$a_{\text{TTT,fig. 7a}} = -\frac{(8192G_N^4 E^3 \pi^4) \omega^4 (d-2) \mathcal{P}_4^3}{8(d-3)^3 (d-1)^4 d^3 (d+1)^2 (d+2)}, \quad (5.19a)$$

$$a_{\text{TTT,fig. 7b}} = \frac{(8192G_N^4 E^3 \pi^4) \omega^6 (d-2) (3d-5) \mathcal{P}_{11}}{12(d-3)^2 (d-1)^4 d (d+1)^2 (d+2) (2d-3) (3d-4) (3d-2)}, \quad (5.19b)$$

$$a_{\text{TTT,fig. 7c}} = -\frac{(8192G_N^4 E^3 \pi^4) \omega^6 (2d-3) \mathcal{P}_4 \mathcal{P}_8}{12(d-3)^2 (d-1)^4 d^2 (d+1)^2 (d+2) (3d-4) (3d-2)}, \quad (5.19c)$$

$$a_{\text{TTT,fig. 7d}} = -\frac{(8192G_N^4 E^3 \pi^4) \omega^6 (2d-3) \mathcal{P}_4 \mathcal{P}_8}{12(d-3)^2 (d-1)^4 d^2 (d+1)^2 (d+2) (3d-4) (3d-2)}, \quad (5.19d)$$

with \mathcal{P}_4 and \mathcal{P}_8 from eq. (4.33) and eq. (5.13) respectively, and

$$\begin{aligned} \mathcal{P}_{11} = & -3024 + 3720d + 2980d^2 + 996d^3 - 2426d^4 - 737d^5 + 799d^6 \\ & - 284d^7 - 36d^8 + 223d^9 - 117d^{10} + 18d^{11}. \end{aligned} \quad (5.20)$$

Assembling the effective action by evaluating the integrals (see appendix B.1), combining with the coefficients, and expanding in $d = 3 + \epsilon$ results in

$$\begin{aligned} S_{\text{TTT}} = & -\frac{214}{525} G_N^4 E^3 \int \frac{d\omega}{2\pi} \omega^8 \kappa_{-+}(\omega) \left\{ \frac{1}{\epsilon^2} + \frac{1}{\epsilon} \left[2 \log \left(\frac{\omega^2 e^{\gamma_E}}{\mu^2 \pi} \right) - 2i\pi \text{sgn}(\omega) - \frac{252583}{29960} \right] \right. \\ & + \left[\log \left(\frac{\omega^2 e^{\gamma_E}}{\mu^2 \pi} \right) \left(2 \log \left(\frac{\omega^2 e^{\gamma_E}}{\mu^2 \pi} \right) - \frac{252583}{14980} \right) + \left(\frac{252583}{14980} - 4 \log \left(\frac{\omega^2 e^{\gamma_E}}{\mu^2 \pi} \right) \right) i\pi \text{sgn}(\omega) \right. \\ & \left. \left. - \frac{29}{2} \zeta_2 - \frac{840}{107} \zeta_3 + \frac{1583459537}{37749600} \right] \right\} \\ & + \epsilon \left[\log \left(\frac{\omega^2 e^{\gamma_E}}{\mu^2 \pi} \right) \left\{ \log \left(\frac{\omega^2 e^{\gamma_E}}{\mu^2 \pi} \right) \left[\frac{4}{3} \log \left(\frac{\omega^2 e^{\gamma_E}}{\mu^2 \pi} \right) - \frac{252583}{14980} \right] \right. \right. \\ & \left. \left. + \left(-29\zeta_2 - \frac{1680\zeta_3}{107} + \frac{1583459537}{18874800} \right) \right\} \right. \\ & + \frac{7324907\zeta_2}{59920} + \frac{14309\zeta_3}{642} + \frac{420\zeta_4}{107} - \frac{104414536729}{634193280} \\ & \left. - i\pi \text{sgn}(\omega) \left\{ 2 \log \left(\frac{\omega^2 e^{\gamma_E}}{\mu^2 \pi} \right) \left(2 \log \left(\frac{\omega^2 e^{\gamma_E}}{\mu^2 \pi} \right) - \frac{252583}{14980} \right) \right. \right. \\ & \left. \left. - 13\zeta_2 - \frac{1680}{107} \zeta_3 + \frac{1583459537}{18874800} \right\} \right] + \mathcal{O}(\epsilon^2) \Bigg\}. \end{aligned} \quad (5.21)$$

We first reported this result in Ref. [47], which was the first time the tail-of-tail-of-tail was tackled outside of traditional GR.

5.3 Tail-of-Tail-of-Tail-of-Tail

Analyzing all of the patterns between the previous tails, we are able to make predictions about both what cuts we need to evaluate, and what their value should be. For the cut

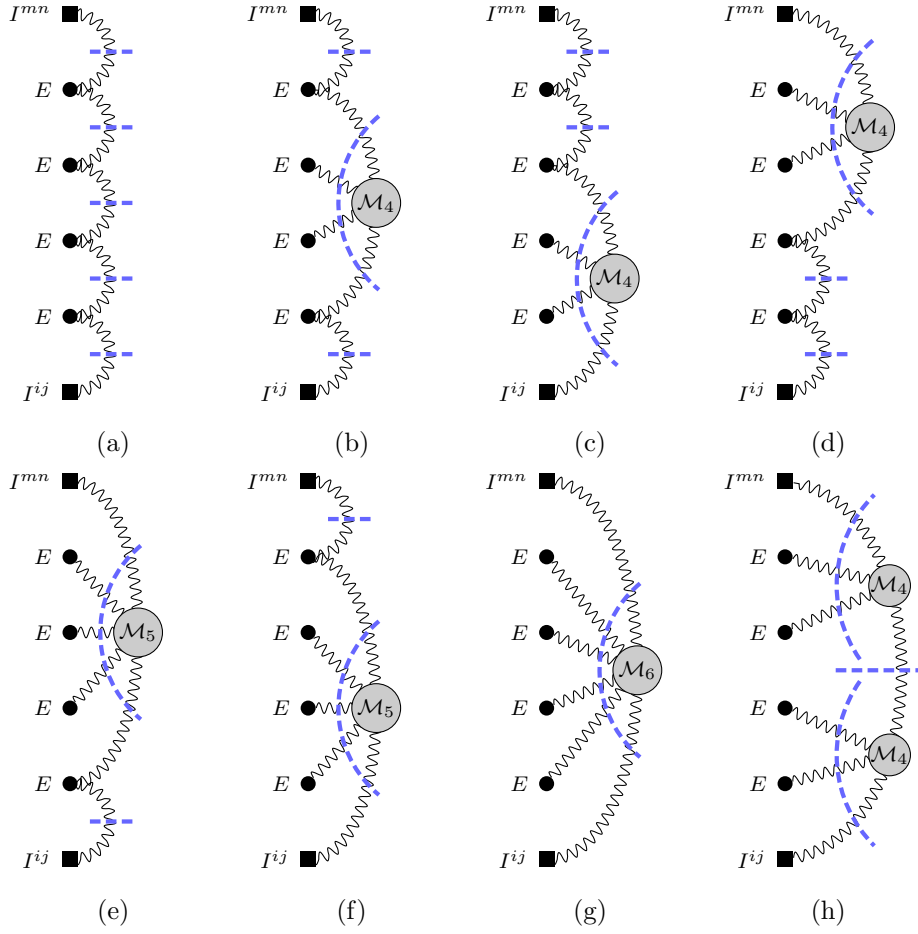


Figure 8: All of the unitarity cut topologies needed for T^4 .

basis, we expect diagrams involving no bulk graviton contacts, as well as all diagrams involving at least four-point bulk contacts. Thus a reasonable initial guess for the needed integrals and cuts would be those shown in figs. 8a to 8g. However, it turns out that this set is slightly incomplete. We use these initial seven diagrams to help define the integral family, with 9 of the $\binom{5}{2} + 5 = 15$ momentum invariants accounted for by the explicit propagators in figs. 8a to 8g via

$$F^{(5)}(\text{fig. 8a}) = F^{(5)}(1, 1, 1, 1, 1, 0, 0, 0, 0, 0, 0, 0, 0, 0, 0) , \quad (5.22a)$$

$$F^{(5)}(\text{fig. 8b}) = F^{(5)}(1, 1, 0, 1, 1, 0, 1, 1, 0, 0, 0, 0, 0, 0, 0) , \quad (5.22b)$$

$$F^{(5)}(\text{fig. 8c}) = F^{(5)}(1, 0, 1, 1, 1, 1, 1, 0, 0, 0, 0, 0, 0, 0, 0) , \quad (5.22c)$$

$$F^{(5)}(\text{fig. 8d}) = F^{(5)}(1, 1, 1, 0, 1, 0, 0, 1, 1, 0, 0, 0, 0, 0, 0) , \quad (5.22d)$$

$$F^{(5)}(\text{fig. 8e}) = F^{(5)}(1, 1, 0, 0, 1, 0, 1, 1, 1, 0, 0, 0, 0, 0, 0) , \quad (5.22e)$$

$$F^{(5)}(\text{fig. 8f}) = F^{(5)}(1, 0, 0, 1, 1, 1, 1, 1, 0, 0, 0, 0, 0, 0, 0) , \quad (5.22f)$$

$$F^{(5)}(\text{fig. 8g}) = F^{(5)}(1, 0, 0, 0, 1, 1, 1, 1, 1, 0, 0, 0, 0, 0, 0) , \quad (5.22g)$$

and the remaining 6 from the internal “planar” potential-mode propagators of \mathcal{M}_6 ⁶. Note that again we are including contributions that can be identified with each other,

$$F^{(5)}(\text{fig. 8b}) = F^{(5)}(\text{fig. 8c}) = F^{(5)}(\text{fig. 8d}), \quad F^{(5)}(\text{fig. 8e}) = F^{(5)}(\text{fig. 8f}), \quad (5.23)$$

so the reflection symmetry considerations mentioned in section 5.2 continue to apply. Checking the basis integrals of this family, we find an eighth relevant basis member, shown in fig. 8h

$$F^{(5)}(\text{fig. 8h}) = F^{(5)}(1, 0, 1, 0, 1, 1, 1, 1, 1, 0, 0, 0, 0, 0, 0). \quad (5.24)$$

This new basis element spoils the one-to-one correspondence between basis integrals and cuts as its propagator structure is a superset of the propagators of fig. 8g. However, it does so in a very mild way: as a cut, fig. 8h is completely contained within $\overline{\text{Cut}}_{\text{fig. 8g}}$ due to factorization. Only the underlying scalar integrals are unrelated. Thus calculating and matching the cut for fig. 8g determines *both* basis coefficients (after taking into account relative symmetry factors).

The explicit rational functions of propagators for each of the cuts is tens of thousands of terms long. The cuts for figs. 8a to 8f and 8h were all just barely computable using a personal computer. Figure 8g required the use of the Quest computing cluster at Northwestern University. For all of the cuts except for fig. 8g, we can observe patterns occurring in the reduced cuts and basis coefficients. Starting with the “all-radiation” cuts, figs. 1b, 3a, 5a and 7a, we see that they follow a simple iteration which suggests that

$$\overline{\text{Cut}}_{\text{fig. 8a}} = (2\pi G_N) \left(\frac{(d+1)(d-2)}{(d+2)(d-1)} \omega^4 \right) \left(\frac{(-8\pi G_N E) \mathcal{P}_4}{(d-3)(d-1)d(d+1)} \right)^4 \prod_{i=1}^5 \delta(Q_i). \quad (5.25)$$

We have verified this prediction through direct calculation of the cut. Similarly, comparing eqs. (5.19c) and (5.19d) to eq. (5.12), we are led to

$$\begin{aligned} \overline{\text{Cut}}_{\text{fig. 8b}} &= \overline{\text{Cut}}_{\text{fig. 8c}} = \overline{\text{Cut}}_{\text{fig. 8d}} \\ &= \frac{(512G_N^3 E^2 \pi^3) \omega^6 (2d-3) \mathcal{P}_8 \left(\frac{(-8\pi G_N E) \mathcal{P}_4}{(d-3)(d-1)d(d+1)} \right)^2}{3(d-3)(d-1)^3 d(d+1)(d+2)(3d-4)(3d-2)}, \end{aligned} \quad (5.26)$$

where from now on the $\delta(Q_i)$ are implicit. These equalities are borne out through explicit computation. Moving on to figs. 8e and 8f, we find that their reduced cuts are

$$\overline{\text{Cut}}_{\text{fig. 8e}} = \overline{\text{Cut}}_{\text{fig. 8f}} = \frac{-(8192G_N^4 E^3 \pi^4) \omega^6 (d-2)(3d-5) \mathcal{P}_{11} \left(\frac{(-8\pi G_N E) \mathcal{P}_4}{2(d-3)(d-1)d(d+1)} \right)}{(d-3)^2 (d-1)^4 d(d+1)^2 (d+2)(2d-3)(3d-4)(3d-2)}, \quad (5.27)$$

yet again in line with an iteration, this time between the tail-type factor and a factor from \mathcal{M}_5 . Figure 8h is the last of the easier cuts. While we mentioned that kinematically it is

⁶Since they do not appear as part of the integral basis, the choice of these propagators is for convenience when handling the intermediate steps during reduction.

contained within fig. 8g, we explicitly include it with the other iterated cuts because it also turns out to be iterative. Specifically, we find that the direct calculation of the cut yields

$$\begin{aligned}\overline{\text{Cut}}_{\text{fig. 8h}} &= \frac{(131072G_N^5 E^4 \pi^5)(2d-3)^2 \omega^8 \mathcal{P}_8^2}{9(d-3)^2(d-2)(d-1)^5 d^2(d+1)^3(d+2)(3d-4)^2(3d-2)^2} \\ &= (2\pi G_N) \left(\frac{(d+1)(d-2)}{(d+2)(d-1)} \omega^4 \right) \left(\frac{(256G_N^2 E^2 \pi^2)(2d-3)\omega^2 \mathcal{P}_8}{3(d-3)(d-2)(d-1)^2 d(d+1)^2(3d-4)(3d-2)} \right)^2,\end{aligned}\quad (5.28)$$

which is the square of eq. (5.12) with an additional prefactor matching the radiation-reaction term eq. (4.18).

Last, we turn our attention to fig. 8g. Since we have already determined fig. 8h, we report only the part of $\overline{\text{Cut}}_{\text{fig. 8g}}$ that dresses $F^{(5)}$ (fig. 8g)

$$\begin{aligned}\overline{\text{Cut}}_{\text{fig. 8g}}|_{F^{(5)}(\text{fig. 8g})} &= \frac{(131072G_N^5 E^4 \pi^5)}{30} \omega^2 \mathcal{P}_{22} \left(\frac{(d+1)(d-2)}{(d+2)(d-1)} \omega^4 \right) \\ &\times \frac{1}{(d-3)^3(d-2)^2(d-1)^4 d^2(d+1)^4(2d-3)(3d-4)^2(3d-2)^2(5d-8)(5d-6)},\end{aligned}\quad (5.29)$$

with

$$\begin{aligned}\mathcal{P}_{22} &= 291600d^{22} - 5364630d^{21} + 43610967d^{20} - 198558153d^{19} + 478961469d^{18} \\ &+ 14340403d^{17} - 4908635433d^{16} + 21042703665d^{15} - 53485147433d^{14} \\ &+ 101573518519d^{13} - 174143104426d^{12} + 309327324244d^{11} - 555238832200d^{10} \\ &+ 944837229872d^9 - 1503589473248d^8 + 2203112130496d^7 - 2911608239232d^6 \\ &+ 3432661203456d^5 - 3454174264320d^4 + 2688616654848d^3 - 1430856658944d^2 \\ &+ 447389982720d - 60914073600.\end{aligned}\quad (5.30)$$

The final piece remaining to assemble the effective action is to enumerate the symmetry factors. Since we are using the over-complete integral basis, all diagrams come with the reflection symmetry factor in addition to the permutation factor for the E coupling

$$\begin{aligned}|G_{\text{fig. 8a}}| &= 2, & |G_{\text{fig. 8b}}| &= |G_{\text{fig. 8c}}| = |G_{\text{fig. 8d}}| = 2 \times 2!, \\ |G_{\text{fig. 8e}}| &= |G_{\text{fig. 8f}}| = 2 \times 3!, & |G_{\text{fig. 8g}}| &= 2 \times 4!, \\ |G_{\text{fig. 8h}}| &= 2 \times (2! \times 2!).\end{aligned}\quad (5.31)$$

The integrals for figs. 8a to 8g are all straightforward to evaluate using the same techniques as the previous calculations. Unfortunately, for fig. 8h we must resort to numerical evaluation and reconstruction, discussed in appendix B.2. Combining all of the above data, expanding in $d = 3 + \epsilon$ and evaluating the CTP sums results in the effective action

contribution

$$\begin{aligned}
S_{\text{TTTT}} = & -\frac{5}{2} \frac{214^2}{525^2} G_N^5 E^4 \int \frac{d\omega}{2\pi} \omega^9 \kappa_{-+}(\omega) \left\{ \frac{i}{\epsilon^2} + \frac{1}{\epsilon} \left[\frac{5}{2} i \log \left(\frac{\omega^2 e^{\gamma_E}}{\mu^2 \pi} \right) + \frac{5\pi \operatorname{sgn}(\omega)}{2} \right. \right. \\
& \left. \left. - i \left(\frac{840}{107} \zeta_2 + \frac{5249287}{343470} \right) \right] \right. \\
& + \left[\frac{5}{2} i \log \left(\frac{\omega^2 e^{\gamma_E}}{\mu^2 \pi} \right) \left(\frac{5}{4} \log \left(\frac{\omega^2 e^{\gamma_E}}{\mu^2 \pi} \right) - \frac{840}{107} \zeta_2 - \frac{5249287}{343470} \right) \right. \\
& + \frac{5}{2} \pi \operatorname{sgn}(\omega) \left(\frac{5}{2} \log \left(\frac{\omega^2 e^{\gamma_E}}{\mu^2 \pi} \right) - \frac{840}{107} \zeta_2 - \frac{5249287\pi \operatorname{sgn}(\omega)}{343470} \right) \\
& \left. + \frac{5541865i\zeta_2}{91592} - \frac{2940}{107} i\zeta_3 - \frac{176400i\zeta_4}{11449} + \frac{90973869743i}{673201200} \right] \\
& \left. + \mathcal{O}(\epsilon^1) \right\}. \tag{5.32}
\end{aligned}$$

This is the first time that the T^4 contribution has been derived in any approach whatsoever in terms of generic quadrupoles.

6 Analysis of Dissipative Sector

The effective actions derived in sections 4 and 5 contain divergences in the dimensional regularization parameter ϵ . The divergences in the dissipative sector, namely of the part of the action that is odd-in- ω , can be handled completely within the tower of tails. This dissipative analysis takes place purely within the “binary-as-composite” EFT at the radiation scale. As mentioned in section 2, the UV (small-scale) theory that defines the quadrupoles, namely the description of the binary dynamics at the orbital scale, allows one to directly compute at sufficiently high PN order the renormalization of the multipole couplings in terms of the IR divergences of the small-scale theory. To highlight that we are focusing on the purely dissipative contributions, we will work at the level of the dissipated energy and energy spectra, ΔE and $\frac{dE}{d\omega}$, respectively. We will then proceed to demonstrate the renormalization of these dissipative contributions up to new subleading orders. We take inspiration from Ref. [26], which is essentially textbook QFT renormalization.

6.1 Energy Loss in the CTP Formalism

The CTP formalism provides a generic extension of Noether’s theorem which accounts for the effects of the non-conservative dynamics on the total energy of the accessible degrees of freedom. Specifically, we have [54]:

$$\frac{dE^{\text{CTP}}}{dt} = -\frac{\partial L}{\partial t} + \dot{q}^I \left[\frac{\partial K}{\partial q_-^I(t)} \right]_{\text{PL}} + \ddot{q}^I \left[\frac{\partial K}{\partial \dot{q}_-^I(t)} \right]_{\text{PL}} + \frac{\partial}{\partial \text{time derivs}} \tag{6.1}$$

for E^{CTP} the energy of the accessible degrees of freedom q . To apply this formula in the case of gravitational tails, we need to analyze the splitting into the conservative and

non-conservative parts of the effective action. Then we must transform the time-domain expression of eq. (6.1) into a frequency-domain.

Splitting the full CTP Lagrangian into the conservative and non-conservative parts only requires knowledge about the functional structure of the generalized coordinates. In the current case of tails, the quadrupoles themselves, $I_{\pm}(\omega)$ (suppressing $SO(3)$ tensor indices in the following discussion), are the relevant generalized coordinates. We have seen in the computations in sections 4 and 5 that the CTP effective actions for the tails take the form:

$$S_{\text{CTP}} = \int_{-\infty}^{\infty} d\omega f(\omega) \kappa_{-+}(\omega), \quad (6.2)$$

in which ω is purely real, but the function $f(\omega)$ may be complex. The conservative part of the CTP effective Lagrangian is defined as the piece expressible as the difference between two distinct histories, which in this case means the part symmetric in the $(-, +)$ variables:

$$\kappa_{\text{C}}(\omega) \equiv \kappa_{11}(\omega) - \kappa_{22}(\omega) \sim \kappa_{-+}(\omega) + \kappa_{+-}(\omega). \quad (6.3)$$

We then adopt an orthogonal change of basis to define:

$$\kappa_{\text{NC}}(\omega) \equiv \kappa_{-+}(\omega) - \kappa_{+-}(\omega), \quad (6.4)$$

so that the CTP effective action becomes:

$$S_{\text{CTP}} = \int_{-\infty}^{\infty} d\omega \left[\frac{1}{2} f(\omega) (\kappa_{\text{C}} + \kappa_{\text{NC}}) \right]. \quad (6.5)$$

Finally, we can use the parity properties of the integral, and $\kappa_{-+}(-\omega) \rightarrow \kappa_{+-}(\omega)$ under $\omega \leftrightarrow -\omega$ to write:

$$S_{\text{CTP}} = \frac{1}{2} \int_{-\infty}^{\infty} d\omega \left[f_{\text{even}}(\omega) \kappa_{\text{C}}(\omega) + f_{\text{odd}}(\omega) \kappa_{\text{NC}}(\omega) \right]. \quad (6.6)$$

We then identify in eq. (6.1) $L(\omega) = \frac{1}{2} f_{\text{even}}(\omega) \kappa_{\text{C}}(\omega)$, and $K(\omega) = \frac{1}{2} f_{\text{odd}}(\omega) \kappa_{\text{NC}}(\omega)$. We assume that the conservative piece does not have an explicit time dependence, and so it does not contribute to eq. (6.1).

In order to apply eq. (6.1) to the Fourier-space non-conservative potential, we need to switch the from frequency dependence in the CTP quadrupole, $I_{-}(\omega)$, back to time dependence via the Fourier transform

$$I_a(\omega) = \int dt e^{-i\omega t} I_a(t), \quad I_a(t) = \frac{1}{2\pi} \int d\omega e^{i\omega t} I_a(\omega). \quad (6.7)$$

This allows to define $K(t)$ as:

$$K(t) = \frac{1}{2} \int d\omega f_{\text{odd}}(\omega) [I_+(\omega) e^{i\omega t} - I_+(-\omega) e^{-i\omega t}] I_-(t), \quad (6.8)$$

and in turn the needed pieces for eq. (6.1) read:

$$\left[\frac{\partial K}{\partial I_-(t)} \right]_{\text{PL}} = \frac{1}{2} \int d\omega f_{\text{odd}}(\omega) (I_+(\omega) e^{i\omega t} - I_+(-\omega) e^{-i\omega t}), \quad (6.9)$$

$$\frac{dI(t)}{dt} = \frac{1}{2\pi} \frac{d}{dt} \int d\omega' e^{i\omega' t} I(\omega') = \frac{1}{2\pi} \int d\omega' (i\omega') e^{i\omega' t} I(\omega'). \quad (6.10)$$

Importantly, this step allows us to ignore terms that contain $I_+(-\omega)I_+(\omega)$ and $I_-(-\omega)I_-(\omega)$, since the first carries no dependence on I_- , and the second vanishes in the physical limit $[\dots]_{\text{PL}}$ after taking the derivative.

We then assemble

$$\begin{aligned}\Delta E &= \int dt \frac{dE^{\text{CTP}}}{dt} \\ &= \frac{1}{2} \frac{1}{2\pi} \int dt d\omega d\omega' (i\omega') e^{i\omega't} I(\omega') f_{\text{odd}}(\omega) [I(\omega) e^{i\omega t} - I(-\omega) e^{-i\omega t}].\end{aligned}\quad (6.11)$$

Resolving the Fourier transforms of the delta functions that arise:

$$\int dt e^{it(\omega+\omega')} = 2\pi\delta(\omega+\omega'), \quad \int dt e^{it(\omega-\omega')} = 2\pi\delta(\omega-\omega'), \quad (6.12)$$

leads to

$$\Delta E = \int d\omega [(-i\omega) f_{\text{odd}}(\omega) \kappa(\omega)]. \quad (6.13)$$

We reiterate that this analysis accounts for the energy change of the binary system, and that the *radiated energy* carried by the gravitational field must, by conservation of energy, be opposite.

6.2 Radiated Energy from Tails

We begin by applying energy loss formula, eq. (6.13), to the CTP effective actions derived in sections 4 and 5. Note that since we have not performed the renormalization at the level of the effective action, these initial energy contributions will still carry dimensional regularization divergences. We will perform the renormalization at the level of the energy loss in the following subsections.

We begin with the radiation reaction term, eq. (4.23). Applying eq. (6.13), we can easily extract the energy loss of the quadrupoles into the gravitational field

$$(\Delta E)_{\text{RR}} = -\frac{G_N}{5\pi} \int_{-\infty}^{\infty} d\omega \kappa(\omega) \omega^6 \left[1 - \frac{\epsilon}{2} \left(\frac{9}{10} - \log \left(\frac{\omega^2 e^{\gamma_E}}{\mu^2 \pi} \right) \right) + \mathcal{O}(\epsilon^2) \right]. \quad (6.14)$$

By energy balance, this must be opposite to the energy carried away by the gravitational field in the form of gravitational waves. The finite part of this energy loss is the Fourier transform of the well-known Einstein quadrupole radiation formula. We present the $\mathcal{O}(\epsilon^1)$ term for later use in renormalization. Similarly, from the tail effective action, eq. (4.35), we compute the energy loss contribution

$$(\Delta E)_{\text{T}} = -\frac{2}{5} G_N^2 E \int_{-\infty}^{\infty} d\omega \kappa(\omega) \omega^7 \left[1 + \epsilon \left(\log \left(\frac{\omega^2 e^{\gamma_E}}{\mu^2 \pi} \right) - \frac{41}{30} \right) + \mathcal{O}(\epsilon^2) \right]. \quad (6.15)$$

This correction is in agreement with previous derivations [24–28, 146], again up to sign conventions.

The energy loss induced from the tail-of-tail comes from eq. (5.15), giving

$$\begin{aligned}
(\Delta E)_{\text{TT}} = & \frac{214G_N^3 E^2}{525\pi} \int_{-\infty}^{\infty} d\omega \kappa(\omega) \omega^8 \left\{ \frac{1}{\epsilon} + \left[\frac{3}{2} \log \left(\frac{\omega^2 e^{\gamma_E}}{\mu^2 \pi} \right) - \frac{420\zeta_2}{107} - \frac{675359}{89880} \right] \right. \\
& + \epsilon \left[\log \left(\frac{\omega^2 e^{\gamma_E}}{\mu^2 \pi} \right) \left(\frac{9}{8} \log \left(\frac{\omega^2 e^{\gamma_E}}{\mu^2 \pi} \right) - \frac{(352800\zeta_2 + 675359)}{59920} \right) \right. \\
& \left. \left. + \frac{4569\zeta_2}{856} - \frac{1050\zeta_3}{107} + \frac{1259125247}{37749600} \right] + \mathcal{O}(\epsilon^2) \right\}. \quad (6.16)
\end{aligned}$$

From T^3 , eq. (5.21), we find

$$\begin{aligned}
(\Delta E)_{\text{TTT}} = & \frac{428}{525} G_N^4 E^3 \int_{-\infty}^{\infty} d\omega \kappa(\omega) \omega^9 \left\{ \frac{1}{\epsilon} + \left[2 \log \left(\frac{\omega^2 e^{\gamma_E}}{\mu^2 \pi} \right) - \frac{252583}{29960} \right] \right. \\
& + \epsilon \left[\log \left(\frac{\omega^2 e^{\gamma_E}}{\mu^2 \pi} \right) \left(2 \log \left(\frac{\omega^2 e^{\gamma_E}}{\mu^2 \pi} \right) - \frac{252583}{14980} \right) \right. \\
& \left. \left. - \frac{13}{2} \zeta_2 - \frac{840}{107} \zeta_3 + \frac{1583459537}{37749600} \right] + \mathcal{O}(\epsilon^2) \right\}. \quad (6.17)
\end{aligned}$$

Finally, the T^4 contribution to the energy loss is computed from eq. (5.32) as

$$\begin{aligned}
(\Delta E)_{\text{TTTT}} = & -\frac{5}{2} \frac{214^2}{525^2 \pi} G_N^5 E^4 \int_{-\infty}^{\infty} d\omega \kappa(\omega) \omega^{10} \left\{ \frac{1}{\epsilon^2} + \frac{1}{\epsilon} \left[\frac{5}{2} \log \left(\frac{\omega^2 e^{\gamma_E}}{\mu^2 \pi} \right) - \frac{840\zeta_2}{107} - \frac{5249287}{343470} \right] \right. \\
& + \left[\frac{5}{2} \log \left(\frac{\omega^2 e^{\gamma_E}}{\mu^2 \pi} \right) \left(\frac{5}{4} \log \left(\frac{\omega^2 e^{\gamma_E}}{\mu^2 \pi} \right) - \frac{840}{107} \zeta_2 - \frac{5249287}{343470} \right) \right. \\
& \left. \left. + \frac{5541865\zeta_2}{91592} - \frac{2940\zeta_3}{107} - \frac{176400\zeta_4}{11449} + \frac{90973869743}{673201200} \right] + \mathcal{O}(\epsilon^1) \right\}. \quad (6.18)
\end{aligned}$$

With the emitted energy contributions computed, we can begin renormalization analysis.

6.3 Going to Subleading RG Flow

The first appearance of a ϵ divergence in the dissipated energy occurs in the tail-of-tail as a simple pole

$$(\Delta E)_{\text{TT}} \Big|_{\epsilon^{-1}} = \frac{2}{3\pi\epsilon} \times \frac{107}{175} G_N^3 E^2 \int_{-\infty}^{\infty} d\omega \omega^8 \kappa(\omega). \quad (6.19)$$

Since no pole appears in the dissipative sector at the tail level, any counterterms and the renormalization must carry a factor of $(G_N E)^2$ to skip tail orders. With this in mind, we introduce a renormalized coupling to the quadrupoles via:

$$\kappa(\omega) \rightarrow \kappa'(\omega) \equiv \kappa(\omega, \mu) \left(1 + \frac{(G_N E)^2 X(\omega)}{\epsilon} + \dots \right), \quad (6.20)$$

where X is an unknown, independent of $(G_N E)^2$ and ϵ , μ is the renormalization scale of the logs, and the ellipsis indicate higher-order terms in $G_N E$. To find X , we substitute

eq. (6.20) into eq. (6.14), and demand that the *total* energy dissipation:

$$(\overline{\Delta E})_{\text{TT}} \equiv [(\Delta E)_{\text{RR}} + (\Delta E)_{\text{T}} + (\Delta E)_{\text{TT}}] \Big|_{\kappa \rightarrow \kappa'} \quad (6.21)$$

is free from ϵ poles up to the TT at order G_N^3 . Notably, since the pole in κ' carries a factor of G_N^2 , the ϵ^{-1} part will only contribute to $(\overline{\Delta E})_{\text{TT}}$ at the appropriate order in G_N via $(\Delta E)_{\text{RR}}$, as $G_N^2((\Delta E)_{\text{T}} + (\Delta E)_{\text{TT}})$ is beyond $\mathcal{O}(G_N^3)$. This pole cancellation requires:

$$X(\omega) = \frac{214}{105}\omega^2 \Rightarrow \kappa'(\omega) \equiv \kappa(\omega, \mu) \left(1 + \frac{214\omega^2(G_N E)^2}{105\epsilon} + \dots \right). \quad (6.22)$$

Moving on to the tail-of-tail-of-tail (T³) we might suspect a new term in κ' carrying G_N^3 . However, performing the explicit calculation using only eq. (6.22), we find:

$$\begin{aligned} (\overline{\Delta E})_{\text{TTT}} = \int_{-\infty}^{\infty} d\omega \kappa(\omega, \mu) & \left[-\frac{\omega^6 G_N}{5\pi} - \frac{2}{5}\omega^7 G_N^2 E \right. \\ & + \frac{1}{\pi} G_N^3 E^2 \omega^8 \left(\frac{214}{525} \log \left(\frac{\omega^2 e^{\gamma E}}{\mu^2 \pi} \right) - \frac{634913}{220500} - \frac{8\zeta_2}{5} \right) \\ & \left. + G_N^4 E^3 \omega^9 \left(\frac{428}{525} \log \left(\frac{\omega^2 e^{\gamma E}}{\mu^2 \pi} \right) - \frac{634913}{110250} \right) + \mathcal{O}(G_N^5) \right], \quad (6.23) \end{aligned}$$

which is also completely free of ϵ poles. This means there is no term in the renormalized coupling, eq. (6.20), of $\mathcal{O}(G_N^3)$. Further terms in eq. (6.20) must only contribute then at G_N^4 , and thus enter via T⁴.

With a renormalized coupling comes a renormalization-group (RG) flow. Using counterterm analysis to determine RG flow equations in gravity is ambiguous due to the presence of topological operators like the Gauss-Bonnet term [147]. Instead, we will study the renormalization-scale dependence of the observable $(\overline{\Delta E})_{\text{TTT}}$ directly. All of the logarithms in $(\overline{\Delta E})_{\text{TTT}}$ carry a renormalization scale μ , that comes from compensating for the misalignment between the mass dimension of G_N , and the required mass dimension of the coupling constant in a dimensionally-regulated action. We also introduced a scale dependence in κ via the renormalization of the source coupling for similar reasons. The RG flow then follows from demanding that $(\overline{\Delta E})_{\text{TTT}}$, a perturbative observable, must be invariant under shifts of the scale:

$$\frac{d}{d\mu} (\overline{\Delta E})_{\text{TTT}} = 0 + \mathcal{O}(G_N^5), \quad (6.24)$$

which leads to the RG equation:

$$\frac{d}{d \log \mu} \kappa(\omega, \mu) = -\frac{428}{105} (G_N E \omega)^2 \kappa(\omega, \mu) + \mathcal{O}(G_N^4), \quad (6.25)$$

$$\Rightarrow \kappa(\omega, \mu) = \left(\frac{\mu}{\mu_0} \right)^{-\frac{428}{105} (G_N E \omega)^2} \kappa(\omega, \mu_0), \quad (6.26)$$

where μ_0 is an arbitrary but fixed reference scale at which κ is measured (or otherwise known, e.g. through a matching calculation with the small-scale theory). This is in exact

agreement with the RG flow originally found by Goldberger and Ross [26], which can be seen by substituting in $\kappa(\omega, \mu) = I_{ij}(-\omega, \mu)I^{ij}(\omega, \mu)$, that introduces a factor of 2 on the LHS of eq. (6.25) but not on the RHS.

With the leading dissipative renormalization dealt with, we now turn to the subleading corrections induced by the TTTT terms. As we saw in eq. (6.18), the unrenormalized $(\Delta E)_{\text{TTTT}}$ has both a double pole, ϵ^{-2} , as well as a single pole. Since we successfully removed the divergence in the construction of $(\overline{\Delta E})_{\text{TTT}}$ with only a G_N^2 counterterm, we know that one of the new terms in κ' must be of the form $Y(G_N E \omega)^4 \epsilon^{-2}$. This term will bring the $\mathcal{O}(G_N)$ term from eqs. (6.14) and (6.23) up to G_N^5 while shifting the ϵ^0 term into a double pole. We find that after adding the new term to κ' , the coefficient of the double pole of $(\overline{\Delta E})_{\text{TTTT}}$ is given by:

$$(\overline{\Delta E})_{\text{TTTT}} \Big|_{\epsilon^{-2}} = \frac{G_N^5 E^4}{5\pi} \int_{-\infty}^{\infty} d\omega \kappa(\omega, \mu) \omega^{10} \left[\underbrace{-Y}_{\text{RR}} + \underbrace{\frac{45796}{11025}}_{\text{TT}} - \underbrace{\frac{22898}{11025}}_{\text{TTTT}} \right]. \quad (6.27)$$

Cancellation of this pole then requires:

$$Y = \frac{22898}{11025} = 2 \frac{107^2}{105^2}, \quad (6.28)$$

in accordance with the expected iteration of the previous counterterm.

However, the iterated counterterm is not the only required correction to κ' . The single pole has been altered, but not completely removed:

$$(\overline{\Delta E})_{\text{TTTT}} \Big|_{\epsilon^{-1}} = \frac{G_N^5 E^4}{5\pi} \times \frac{1695233}{105^3} \int_{-\infty}^{\infty} d\omega \kappa(\omega, \mu) \omega^{10}. \quad (6.29)$$

Removing this pole necessitates a second new term in κ' of the form $Z(G_N E \omega)^4 \epsilon^{-1}$. Incorporating this new correction to $(\overline{\Delta E})_{\text{TTTT}}$ will allow the finite piece of RR, eq. (6.14), to also contribute a ϵ^{-1} pole at G_N^5 . We then find that $Z = \frac{1695233}{105^3}$. Thus, with two new terms, κ' becomes:

$$\kappa'(\omega) \equiv \kappa(\omega, \mu) \left(1 + 2 \left(\frac{107}{105} \frac{(G_N E \omega)^2}{\epsilon} + \frac{107^2}{105^2} \frac{(G_N E \omega)^4}{\epsilon^2} \right) + \frac{1695233}{105^3} \frac{(G_N E \omega)^4}{\epsilon} + \dots \right), \quad (6.30)$$

and the inclusive energy loss is:

$$\begin{aligned} (\overline{\Delta E})_{\text{TTTT}} = & (\overline{\Delta E})_{\text{TTT}} + \frac{G_N^5 E^4}{5\pi} \int_{-\infty}^{\infty} d\omega \kappa(\omega, \mu) \omega^{10} \left\{ 32\zeta_4 + 2^4 \frac{107}{105} \zeta_3 - \frac{1132438}{105^2} \zeta_2 \right. \\ & - \frac{275977249}{1944810} - 2 \frac{107^2}{105^2} \log^2 \left(\frac{\omega^2 e^{\gamma_E}}{\mu^2 \pi} \right) \\ & \left. + \log \left(\frac{\omega^2 e^{\gamma_E}}{\mu^2 \pi} \right) \left[\frac{8301847}{257250} + 2^4 \frac{107}{105} \zeta_2 \right] \right\}. \quad (6.31) \end{aligned}$$

Since the TTTT energy loss required a new counterterm (and has a subleading log), there will be a new term in the RG flow associated to it. We again simply demand that:

$$\frac{d}{d\mu}(\overline{\Delta E})_{\text{TTTT}} = 0 + \mathcal{O}(G_N^6), \quad (6.32)$$

which leads to the RG equation:

$$\frac{d}{d \log \mu} \kappa(\omega, \mu) = -(2G_N E \omega)^2 \kappa(\omega, \mu) \left(\frac{107}{105} + \frac{1695233}{105^3} (G_N E \omega)^2 \right) + \mathcal{O}(G_N^5). \quad (6.33)$$

This new RG equation necessarily includes the leading RG flow, and now allows for prediction of subleading logs at all higher-order tails.

7 Post-Newtonian and Self-Force Results

In this section, we present comparisons of our energy loss with those derived via traditional GR results in PN and self-force theory for further checks that go beyond the tail. Observable results from these GR approaches are presented in a PN expansion, eventually specified to a quasi-circular orbit. Our results are also in the PN regime due to the multipole expansion of the inspiral. Thus, matching against the known PN results primarily entails inserting a PN-expanded quadrupole expression, and then aligning related scheme choices.

7.1 PN Mapping to the Binary Inspiral

We will focus on the leading PN expansion, which for a binary system is simply a circular orbit. WLOG, we take the circular orbit to be in the x - y plane, in which the frequency-space quadrupole components can be chosen as

$$\begin{aligned} I_{xx}(\omega) &= I_{yy}(\omega) = \nu E r^2 \pi / 2 (\delta(\omega - 2\Omega) + \delta(\omega + 2\Omega)), \\ I_{xy}(\omega) &= I_{yx}(\omega) = -i \nu E r^2 \frac{\pi}{2} (\delta(\omega - 2\Omega) - \delta(\omega + 2\Omega)), \\ I_{zj}(\omega) &= 0, \end{aligned} \quad (7.1)$$

with ω the radiation frequency, $\Omega > 0$ the orbital frequency, r the radius of the circular orbit, ν the symmetric mass ratio of the binary, and E the energy of the binary. From these expressions, we easily arrive at the quadrupole-quadrupole “two-point” contraction:

$$\kappa(\omega) = E^2 \pi^2 r^4 \nu^2 (\delta(\omega - 2\Omega)^2 + \delta(\omega + 2\Omega)^2). \quad (7.2)$$

Upon integration in ω , the $\delta(\omega \pm 2\Omega)^2$ will leave behind a $\delta(0)$. These are resolved by noting that the PN energy loss for the binary is actually computed as the time-averaged energy loss of the system over a sufficiently long period of time [13]. Invoking one of the definitions of the frequency space $\delta(0)$,

$$\delta(0) \equiv \lim_{T \rightarrow \infty} \frac{1}{2\pi} \int_{-T/2}^{T/2} e^{-it0} dt = \lim_{T \rightarrow \infty} \frac{T}{2\pi}, \quad (7.3)$$

we can formally align the time-averaging interval with the T in eq. (7.3), canceling said T dependence from the final result. The net result is that we can effectively use

$$\kappa(\omega) = \frac{E^2 \pi r^4 \nu^2}{2} (\delta(\omega - 2\Omega) + \delta(\omega + 2\Omega)) \quad (7.4)$$

as the quadrupole contraction in order to match against the PN results.

We will also eventually need Kepler's law, $GE/r = (r\Omega)^2$, to rewrite expressions in terms of the PN parameter $x \equiv (GE\Omega)^{2/3}$. All of the above are leading-order expressions in the PN expansion, which have subleading corrections that we ignore here. These leading expressions are sufficient for us to verify critical features of our results: the leading logs and leading transcendental numbers.

7.2 Direct Comparisons

We begin by looking at the radiation-reaction and the tail. Since these actions contain no divergences or logarithms in their dissipative part, there is no subtlety about aligning choices of logarithm scales. Thus, we simply insert eq. (7.4) into eqs. (6.14) and (6.15) which gives:

$$(\overline{\Delta E})_{G_N, G_N^2}^{\text{LO PN}} = -\frac{32x^5 \nu^2}{5G_N} - \frac{256\pi x^{13/2} \nu^2}{5G_N} + \dots \quad (7.5)$$

in agreement (up to the energy balance sign) with the long-known results of Blanchet and Damour [13, 24, 146].

For higher-order tails, we need to carefully process the total PN energies, including the renormalization of the quadrupoles, and align subtraction schemes. The RG flows from section 6.3 trade out dependence on $\log(\mu)$, the renormalization flow parameter, for $\log(\mu_0)$, the scale at which we perform EFT matching to the short-scale theory, the orbital separation r in our case. Thus we take $\mu_0^{-1} \rightarrow r$. A proportionality constant is left undetermined, and amounts to different choices of subtraction scheme, which we consider next.

We must align subtraction schemes between our results and traditional GR literature. In section 6, the counterterms we introduced only absorbed the divergences, and not any additional constants. Thus we are technically working in a pure minimal subtraction scheme. However, we have explicitly packaged the logarithms into $\log \frac{\omega^2 \exp(\gamma_E)}{\mu^2 \pi}$, which makes it easy to switch to $\overline{\text{MS}}$ subtraction by sending $\mu^2 \rightarrow \frac{\exp(\gamma_E)}{4\pi} \mu^2$, or to other nonstandard schemes via similar replacements. For the TT and TTT, we compare against the work of Blanchet et al [13, 30, 31, 148, 149], whose results include γ_E but not $\log \pi$, suggesting that their implicit renormalization scheme is not equivalent to either MS or $\overline{\text{MS}}$. We will thus adopt a generic subtraction via $\mu^2 \rightarrow A\pi^{-1}\mu^2$, and determine the proper choice of A to align schemes.

Pushing our $\mathcal{O}(G_N^3)$ term from eq. (6.23) through the transformation to PN variables, including the generic subtraction and renormalization considerations, we arrive at:

$$(\overline{\Delta E})_{G_N^3}^{\text{LO PN}} \rightarrow -\frac{32}{5G_N} \nu^2 x^8 \left[\frac{634913}{11025} + 32\zeta_2 - \frac{856}{105} (\log x + 2 \log 2 + \gamma_E - \log A) \right]. \quad (7.6)$$

Comparing with known PN results [13, 30, 31, 148, 149]

$$\mathcal{F}_{\nu^2 x^8} = \frac{32}{5G_N} \nu^2 x^8 \left[\frac{6643739519}{69854400} + 32\zeta_2 - \frac{856}{105} (\log x + 4 \log 2 + 2\gamma_E) \right]. \quad (7.7)$$

The $\log x$ terms match exactly, up to the energy balance sign. Since all of the transcendental numbers are newly-appearing at this order, we expect to also match them exactly up to choice of subtraction scheme and the energy balance sign. We see that choosing a subtraction scheme with $A = (4 \exp(\gamma_E))^{-1}$ leads to the desired matching. Note that this subtraction scheme is equivalent to using a dimensionally-regulated gravitational constant:

$$\mu^2 \rightarrow \frac{\mu^2}{4\pi e^{\gamma_E}} \Rightarrow G_N \rightarrow G_d \equiv G_N \left(\frac{\sqrt{4\pi e^{\gamma_E}}}{\mu} \right)^{d-3}, \quad (7.8)$$

which is also motivated by PN calculations in the conservative sector, see for instance Refs. [78, 150]. Matching the rational number would require inserting the higher-order PN terms of $\kappa(\omega)$ (as well as E) into the RR contribution, which would allow the rational terms at $\mathcal{O}(G_N)$ to contribute at $\mathcal{O}(x^8)$.

Similarly, we extract the PN terms coming from our $\mathcal{O}(G_N^4)$ contribution to eq. (6.23) using the above fixed subtraction scheme:

$$(\overline{\Delta E})_{G_N^4}^{\text{LO PN}} \rightarrow -\frac{32}{5G_N} \nu^2 x^{19/2} 4\pi \left[\frac{634913}{11025} - \frac{856}{105} (\log x + 4 \log 2 + 2\gamma_E) \right], \quad (7.9)$$

and compare against the known PN result [31]:

$$\mathcal{F}_{\nu^2 x^{19/2}} = \frac{32}{5G_N} \nu^2 x^{19/2} 4\pi \left[\frac{265978667519}{2980454400} - \frac{856}{105} (\log x + 4 \log 2 + 2\gamma_E) \right], \quad (7.10)$$

with which we again find agreement between all terms, except for the rational contribution, where the piece from TTT is partial to the full PN correction.

For T^4 , the only available results are from self-force theory. Results at the appropriate order we need here are available in Refs. [55, 56], written in terms of the orbit velocity $v \sim x^{1/2}$. With our leading quadrupole in the PN expansion we should exactly match terms like ζ_4 and $\log^2 x$. The $\log 3$ and $\log 5$ come from higher-order multipoles, while the other terms receive contributions from higher-order PN terms in the quadrupole bringing terms from RR and TT up to $x^{11} \sim v^{22}$. We organize the results so that the terms we should match appear first, the ones that we cannot appear later, and we ignore completely the $\log 3$ and $\log 5$ terms from Refs. [55, 56]. From our results in eq. (6.31), we obtain:

$$\begin{aligned} (\overline{\Delta E})_{G_N^5}^{\text{LO PN}} = & -\frac{32}{5G_N} \nu^2 v^{22} \left[-512\zeta_4 - \frac{27392}{105}\zeta_3 + \frac{1465472}{11025} (\log(v) + \gamma_E + 2 \log 2)^2 \right. \\ & - \frac{54784}{105}\zeta_2 (\log v + \gamma_E + 2 \log 2) \\ & + \frac{2207817992}{972405} - \frac{132829552}{128625}\gamma_E - \frac{265659104}{128625} \log 2 - \frac{132829552}{128625} \log v \\ & \left. + \frac{18119008}{11025}\zeta_2 \right], \end{aligned} \quad (7.11)$$

which we compare against the expressions from Refs. [55, 56]:

$$\begin{aligned}
\frac{dE^{(12)}}{dt} = & \left(\frac{dE}{dt} \right)_N \left[-512\zeta_4 - \frac{27392}{105}\zeta_3 + \frac{1465472}{11025}(\log(v) + \gamma_E + 2\log 2)^2 \right. \\
& - \frac{54784}{105}\zeta_2(\log v + \gamma_E + 2\log 2) \\
& + \frac{2067586193789233570693}{602387400044430000} - \frac{246137536815857}{157329572400}\gamma_E \\
& - \frac{271272899815409}{157329572400}\log 2 - \frac{246137536815857}{157329572400}\log v \\
& \left. + \frac{3803225263}{1746360}\zeta_2 \right]. \tag{7.12}
\end{aligned}$$

We find that all of the terms match as expected, namely the first two lines in both expressions.

8 Conclusions

In this paper we presented in detail a novel methodology to treat higher-order non-linear effects of gravitational radiation that is scattered from binary inspirals, where conservative and dissipative dynamics are inevitably intertwined. The primary new idea that was first introduced in [47], and enabled our uniquely distinct approach to these type of effects, is that we make our analysis directly at level of the whole binary taken as a single composite particle interacting with gravity. This distinguishes our current line of study from all the many amplitudes-driven works, which study the unbound 2-to-2 scattering problem rather than the actual bound two-body problem which is the primary focus of present and planned GW experiments.

We treat the l -th multipole moments of the whole radiating binary coupled to gravity in the EFT of the composite particle in analogy to massive elementary particles of spin $l/2$ and their gravitational scattering amplitudes. In this paper we go one step forward in grounding our approach, where in section 4.1 we start from pure tree amplitudes as our analogous building blocks from which we construct the necessary unitarity cuts, rather than using the EFT vertices as a given. We verified that these pure amplitude replacements work through to the highest orders reached in the present work. In section 4, we spelled out our new method for the well-studied lower-order effects of radiation-reaction and tail, where the CTP formalism adopted to our problem is layered on top of our integral basis and generalized-unitarity inspired procedure.

In view of the pressing need to push such predictions to high PN orders, we proceeded in section 5 to study higher-order tails all through to the third subleading tail effect: This is the 5-loop tail-of-tail-of-tail-of-tail, or T^4 , at order G^5 corresponding to 8.5PN. One interesting benefit of our method is that it naturally organizes the results at each tail level according to an iterative pattern. We pointed out explicit examples for the cut coefficients in section 5.3. However, there are other interesting hints at iterative and recursive structure. For instance, the number of *actually distinct* cut diagrams and contributions at each tail

order so far tracks the Fibonacci sequence:

$$\text{RR} \rightarrow 1 \quad \text{T} \rightarrow 1 \quad \text{TT} \rightarrow 2 \quad \text{TTT} \rightarrow 3 \quad \text{T}^4 \rightarrow 5. \quad (8.1)$$

It would be interesting to explore these patterns and attempt to identify a structure which directly produces the various cut coefficients.

Let us highlight that also in contrast with all other amplitudes-driven related studies, we only deal with classical propagating gravitons, and land directly on causal effective actions, which encompass the full conservative and dissipative dynamics of these effects. For the lower-order results in section 4, these could be checked against previous EFT results [27, 88]. However, as of the TT level the causal effective actions we obtained in our approach in section 5 have never been previously derived. Yet, in section 6 after we formulate the consequent energy loss of the tails, we could verify through a renormalization analysis that the related leading RG flow of the quadrupole coupling is in perfect agreement with that of [26], where only the TT level was reached.

Additionally, the new T^4 corrections we obtained to the effective action, eq. (5.32), and its associated correction to the emitted energy, eq. (6.18), led us to identify a novel counterterm in the quadrupole coupling, eq. (6.30), and an associated new term in the RG flow of the renormalized quadrupoles, eq. (6.33). Because the new effects continue the pattern of skipping loop orders, it would be interesting to check our results by computing the T^5 contributions, which should produce the same counterterms and RG flows. Beyond that we could only establish that our energy emissions are consistent with those derived via traditional PN-theory results [13, 31], available only up through T^3 , as well as specific pieces of the results from self-force theory [55, 56].

Acknowledgments

We thank John Joseph Carrasco, Sasank Chava, and Radu Roiban for feedback on the manuscript. AE is supported by the USDOE under contract DE-SC0015910 and by Northwestern University via the Amplitudes and Insight Group, Department of Physics and Astronomy, and Weinberg College of Arts and Sciences. ML has been supported by the Science and Technology Facilities Council (STFC) Rutherford Grant ST/V003895 “*Harmonising QFT for Gravity*”, and by the Mathematical Institute University of Oxford.

This research was supported in part through the computational resources and staff contributions provided for the Quest high performance computing facility at Northwestern University which is jointly supported by the Office of the Provost, the Office for Research, and Northwestern University Information Technology.

fillT_EXwas used as part of writing the bibliography [151].

A Handling Tensor Reductions

Throughout our tail calculations, we encounter cuts which are functions of the loop momenta ℓ_x , the radiation frequency ω and the Euclidean metric δ^{op} with four Euclidean

indices contracted against the quadrupoles,

$$\mathcal{N}^{ij;mn}(\{\ell_x, \omega\}) I^{ij}(\omega) I^{mn}(-\omega) , \quad (\text{A.1})$$

that will require tensor reduction to reach the final state factor $\kappa(\omega) = I^{ij}(-\omega) I^{ij}(\omega)$. While we could perform this reduction term-by-term at the level of the individual numerator and propagator combinations that appear, this order of processing delays the introduction of ℓ^2 that should be zeroed by on-shell conditions in the construction of the cut. We will instead introduce a generic tensor reduction scheme that can easily be applied during the process of cut assembly by constructing a tensor $\mathbf{U}^{ij;mn}$ such that

$$\mathcal{N}^{ij;mn} I^{ij} I^{mn} = \mathcal{N}^{ij;mn} \mathbf{U}^{ij;mn} \kappa(\omega) , \quad (\text{A.2})$$

subject to the symmetry and trace constraints

$$\mathbf{U}^{ij;mn} = \mathbf{U}^{ji;mn} = \mathbf{U}^{ij;nm} , \quad (\text{A.3})$$

$$\mathbf{U}^{ii;mn} = \mathbf{U}^{ij;mm} = 0 . \quad (\text{A.4})$$

With the spatial Euclidean metric as the only available (even-parity) tensor to construct \mathbf{U} from, we find a unique object

$$\mathbf{U}^{ij;mn} = -2 \frac{\delta^{ij} \delta^{mn}}{(d+2)d(d-1)} + \frac{\delta^{im} \delta^{jn} + \delta^{in} \delta^{jm}}{(d+2)(d-1)} . \quad (\text{A.5})$$

We can then insert eq. (A.2) during the evaluation of a cut, after splitting the four-momenta into frequencies and spatial momenta.

We have explicitly checked that this method reproduces the term-by-term reduction method for a number of integrals relevant to the tails.

B Evaluating Basis Integrals

B.1 Analytic Evaluation and Bubble Iteration

The two most important integrals we need for evaluating all of the basis integrals appear in Chapter 10 of Smirnov’s *Analytic Tools for Feynman Integrals* [125]. Important to note is that Ref. [125] works in mostly-minus Minkowski signature, whereas the integrals we need to evaluate are in Euclidean signature. To compensate for this, we need to Wick rotate the Minkowski integrals to Euclidean signature via $\ell_0 \rightarrow i\ell_E$ which takes $\ell^2 \rightarrow -\ell_E^2$ and $d^d\ell \rightarrow i d^d\ell_E$. The i from the change in measure cancels against the i as part of the $i\pi^{d/2}$ normalization, and the change-in-sign of the propagators will induce an extra phase $(-1)^\lambda$ for each propagator, as well as *change the relative sign* between ℓ^2 and m^2 for the massive propagators. For example, the massive one-propagator integral, the “tadpole”, in Minkowski signature is

$$\int \frac{d^d k}{(-k^2 + m^2)^\lambda} = i\pi^{d/2} \frac{\Gamma(\lambda - d/2)}{\Gamma(\lambda)} \frac{1}{(m^2)^{\lambda - d/2}} . \quad (\text{B.1})$$

Switching to Euclidean signature, we get

$$\int_E \frac{d^d k_E}{(-k_E^2 - m^2)^\lambda} = (-1)^\lambda \pi^{d/2} \frac{\Gamma(\lambda - d/2)}{\Gamma(\lambda)} \frac{1}{(m^2)^{\lambda - d/2}}. \quad (\text{B.2})$$

From here on, we drop the explicit E label on the integrated momenta. The scale of the tadpole integrals that actually occurs throughout the basis integrals used in section 4 is really the graviton frequency ω^2 , and always appears with the opposite sign compared with an actual mass as in eq. (B.2). In addition, we need to switch to the physical π normalization. Thus, the integral we need for evaluation is

$$F^{(1)}(\lambda; \omega^2) = G^{(1)}(\lambda) = \int_E \frac{d^d k}{(2\pi)^d} \frac{1}{(-k^2 - (-\omega^2))^\lambda} = \frac{\Gamma(\lambda - d/2)}{\Gamma(\lambda)} \frac{(-1)^\lambda (4\pi)^{-d/2}}{(-\omega^2)^{\lambda - d/2}}, \quad (\text{B.3})$$

where we have suppressed the explicit $i0$ component of ω because *we are not integrating over it as part of $d^d k$* .

Similarly, the $m_1 = m_2 = m, m_3 = 0$ two-loop three-propagator integral in Euclidean signature is given by

$$\begin{aligned} & \int_E \frac{d^d k \, d^d l}{(-k^2 - m^2)^{\lambda_1} (-l^2 - m^2)^{\lambda_2} [-(k+l)^2]^{\lambda_3}} \\ &= (\pi^{d/2})^2 (-1)^{\lambda_1 + \lambda_2 + \lambda_3} \frac{\Gamma(\lambda_1 + \lambda_3 - d/2) \Gamma(\lambda_2 + \lambda_3 - d/2) \Gamma(d/2 - \lambda_3)}{\Gamma(\lambda_1) \Gamma(\lambda_2)} \\ & \times \frac{\Gamma(\lambda_1 + \lambda_2 + \lambda_3 - d)}{\Gamma(\lambda_1 + \lambda_2 + 2\lambda_3 - d) \Gamma(d/2) (m^2)^{\lambda_1 + \lambda_2 + \lambda_3 - d}} \\ &= (\pi^{d/2})^2 (-1)^{\lambda_1 + \lambda_2 + \lambda_3} B_{\lambda_1, \lambda_2, \lambda_3; d} (m^2)^{-\lambda_1 - \lambda_2 - \lambda_3 + d}. \end{aligned} \quad (\text{B.4})$$

As in the case of the tadpole, the basis integrals we encounter have the opposite relative sign between k^2 and ω^2 , meaning instead we are interested in

$$G^{(2)}(\lambda_1, \lambda_2, \lambda_3) = (4\pi)^{-d} (-1)^{\lambda_1 + \lambda_2 + \lambda_3} B_{\lambda_1, \lambda_2, \lambda_3; d} (-\omega^2)^{-\lambda_1 - \lambda_2 - \lambda_3 + d}. \quad (\text{B.5})$$

The generic bubble integral is also useful as an intermediate step, namely

$$\begin{aligned} \int_E \frac{d^d k}{(2\pi)^d} \frac{1}{(-k^2)^{\lambda_1} [-(q-k)^2]^{\lambda_2}} &= \frac{(-1)^{d/2}}{(4\pi)^{d/2}} \frac{\Gamma(d/2 - \lambda_1) \Gamma(d/2 - \lambda_2) \Gamma(\lambda_1 + \lambda_2 - d/2)}{\Gamma(\lambda_1) \Gamma(\lambda_2) \Gamma(d - \lambda_1 - \lambda_2) (-q_E^2)^{\lambda_1 + \lambda_2 - d/2}} \\ &= (-1)^{d/2} (4\pi)^{-d/2} A_{\lambda_1, \lambda_2; d} (-q_E^2)^{-\lambda_1 - \lambda_2 + d/2}. \end{aligned} \quad (\text{B.6})$$

Importantly, the Euclidean bubble produces a new Euclidean propagator, and matching the sign choice for this new propagator to the one used for integration absorbs the ubiquitous phase $(-1)^{\lambda_1 + \lambda_2}$. Note that, as expected from the topology, the expression is symmetric in λ_1 and λ_2 .

With these ingredients, we can begin evaluating the higher-loop basis integrals recursively. The first non-trivial integral we need to evaluate is the TT bulk contact integral, $F^{(3)}(1, 1, 1, 1, 0, 0)$ from eq. (4.26). The two potential mode propagators can be integrated together as a bubble using eq. (B.6) with $q = \ell_1 + \ell_3$, resulting in a single new potential

mode propagator. The remaining integral is now of the form eq. (B.4), with a shifted index on the scaleless propagator. Putting everything together, we have

$$\begin{aligned} F^{(3)}(1, 1, 1, 1, 0, 0) &= (-1)^{d/2} (4\pi)^{-d/2} A_{1,1;d} G^{(2)}(1, 1, 2 - d/2) \\ &= (4\pi)^{-3d/2} A_{1,1;d} B_{1,1,2-d/2;d} (-\omega^2)^{-4+3d/2}. \end{aligned} \quad (\text{B.7})$$

This expression is readily expandable near $d = 3$. Evaluating the TTT and T^4 bulk contacts proceeds in a similar manner, just with more levels of bubble iteration, yielding

$$\begin{aligned} F^{(4)}(\text{fig. 7b}) &= (-1)^d (4\pi)^{-d} A_{1,1;d} A_{1,2-d/2;d} G^{(2)}(1, 1, 3 - d) \\ &= (4\pi)^{-2d} A_{1,1;d} A_{1,2-d/2;d} B_{1,1,3-d;d} (-\omega^2)^{-5+2d}, \end{aligned} \quad (\text{B.8})$$

$$F^{(5)}(\text{fig. 8g}) = (4\pi)^{-5d/2} A_{1,1;d} A_{1,2-d/2;d} A_{1,3-d;d} B_{1,1,4-3d/2;d} (-\omega^2)^{-6+5d/2}. \quad (\text{B.9})$$

B.2 Evaluation of Figure 8h

We do not know of a way to analytically evaluate the T^4 integral corresponding to the $\mathcal{M}_4 \otimes \mathcal{M}_4$ topology, fig. 8h. However, we can exploit the fact that, like all the other integrals we consider, the ω^2 scale of the integral is completely factorizable

$$F^{(5)}(\text{fig. 8h}) \equiv (-\omega^2)^{5d/2-7} \mathcal{I}_{4\otimes 4}(1), \quad (\text{B.10})$$

so that we just need to numerically determine $\mathcal{I}_{4\otimes 4}(1)$ as an expansion in the dimensional regularization parameter. We use the program AMFlow [152] in conjunction with Kira [153] to evaluate $\mathcal{I}_{4\otimes 4}(1)$ up to $\mathcal{O}(\epsilon^2)$ with 500 digits of precision at each order. We can then use the PSLQ algorithm [154, 155] to reconstruct the transcendental numbers, using the transcendental numbers appearing in the other T^4 integrals as a guide for guessing the basis. We find, using AMFlow's definition of $d = 3 - 2\epsilon$ instead of the $d = 3 + \epsilon$ that we use in the rest of the paper,

$$\begin{aligned} \mathcal{I}_{4\otimes 4}(1) &= \frac{1}{8(4\pi)^5} \left[\frac{1}{\epsilon^2} + \frac{16 + 5(\log(\pi) - \gamma_E)}{\epsilon} \right. \\ &\quad + (184 + 80(\log(\pi) - \gamma_E) + \frac{25}{2}(\log(\pi) - \gamma_E)^2 + \frac{47}{2}\zeta_2) \\ &\quad + \epsilon \left(1888 + 920(\log(\pi) - \gamma_E) + 200(\log(\pi) - \gamma_E)^2 + \frac{125}{6}(\log(\pi) - \gamma_E)^3 \right. \\ &\quad \left. \left. + 408\zeta_2 - \frac{611}{3}\zeta_3 + \frac{235}{2}\zeta_2(\log(\pi) - \gamma_E) \right) \right. \\ &\quad \left. \epsilon^2 \left(18544 + 9440(\log(\pi) - \gamma_E) + 2300(\log(\pi) - \gamma_E)^2 \right. \right. \\ &\quad \left. \left. + \frac{1000}{3}(\log(\pi) - \gamma_E)^3 + \frac{625}{24}(\log(\pi) - \gamma_E)^4 \right. \right. \\ &\quad \left. \left. + 5092\zeta_2 + 2040\zeta_2(\log(\pi) - \gamma_E) + \frac{1175}{4}\zeta_2(\log(\pi) - \gamma_E)^2 \right. \right. \\ &\quad \left. \left. + \frac{42193}{40}\zeta_2^2 - \frac{9872}{3}\zeta_3 - \frac{3055}{3}\zeta_3(\log(\pi) - \gamma_E) \right) + \mathcal{O}(\epsilon^3) \right]. \end{aligned} \quad (\text{B.11})$$

We have verified the reconstruction using an additional numerical evaluation in AMFlow to 1000 digits. This depth in the ϵ expansion is more than sufficient, after matching ϵ conventions, to obtain up through the $\mathcal{O}(\epsilon^0)$ part of the T^4 effective action.

References

- [1] LIGO SCIENTIFIC, VIRGO collaboration, B. P. Abbott et al., *Observation of Gravitational Waves from a Binary Black Hole Merger*, *Phys. Rev. Lett.* **116** (2016) 061102 [[1602.03837](#)].
- [2] LIGO SCIENTIFIC, VIRGO collaboration, B. P. Abbott et al., *GW151226: Observation of Gravitational Waves from a 22-Solar-Mass Binary Black Hole Coalescence*, *Phys. Rev. Lett.* **116** (2016) 241103 [[1606.04855](#)].
- [3] LIGO SCIENTIFIC, VIRGO collaboration, B. P. Abbott et al., *GW170817: Observation of Gravitational Waves from a Binary Neutron Star Inspiral*, *Phys. Rev. Lett.* **119** (2017) 161101 [[1710.05832](#)].
- [4] LIGO SCIENTIFIC, VIRGO collaboration, B. P. Abbott et al., *GW170104: Observation of a 50-Solar-Mass Binary Black Hole Coalescence at Redshift 0.2*, *Phys. Rev. Lett.* **118** (2017) 221101 [[1706.01812](#)].
- [5] LIGO SCIENTIFIC, VIRGO collaboration, B. P. Abbott et al., *GW170814: A Three-Detector Observation of Gravitational Waves from a Binary Black Hole Coalescence*, *Phys. Rev. Lett.* **119** (2017) 141101 [[1709.09660](#)].
- [6] LIGO SCIENTIFIC, VIRGO collaboration, B. P. Abbott et al., *GW170608: Observation of a 19-solar-mass Binary Black Hole Coalescence*, *Astrophys. J. Lett.* **851** (2017) L35 [[1711.05578](#)].
- [7] LIGO SCIENTIFIC collaboration, J. Aasi et al., *Advanced LIGO*, *Class. Quant. Grav.* **32** (2015) 074001 [[1411.4547](#)].
- [8] VIRGO collaboration, F. Acernese et al., *Advanced Virgo: a second-generation interferometric gravitational wave detector*, *Class. Quant. Grav.* **32** (2015) 024001 [[1408.3978](#)].
- [9] KAGRA collaboration, T. Akutsu et al., *Overview of KAGRA: Detector design and construction history*, *PTEP* **2021** (2021) 05A101 [[2005.05574](#)].
- [10] P. Amaro-Seoane, H. Audley, S. Babak, J. Baker, E. Barausse, P. Bender et al., *Laser Interferometer Space Antenna*, *arXiv e-prints* (2017) arXiv:1702.00786 [[1702.00786](#)].
- [11] D. Reitze et al., *Cosmic Explorer: The U.S. Contribution to Gravitational-Wave Astronomy beyond LIGO*, *Bull. Am. Astron. Soc.* **51** (2019) 035 [[1907.04833](#)].
- [12] M. Maggiore et al., *Science Case for the Einstein Telescope*, *JCAP* **03** (2020) 050 [[1912.02622](#)].
- [13] L. Blanchet, *Gravitational Radiation from Post-Newtonian Sources and Inspiralling Compact Binaries*, *Living Rev. Rel.* **17** (2014) 2 [[1310.1528](#)].
- [14] D. Bini, T. Damour and A. Geralico, *Novel approach to binary dynamics: application to the fifth post-Newtonian level*, *Phys. Rev. Lett.* **123** (2019) 231104 [[1909.02375](#)].
- [15] D. Bini, T. Damour and A. Geralico, *Binary dynamics at the fifth and fifth-and-a-half post-Newtonian orders*, *Phys. Rev. D* **102** (2020) 024062 [[2003.11891](#)].
- [16] D. Bini, T. Damour, A. Geralico, S. Laporta and P. Mastrolia, *Gravitational dynamics at $O(G^6)$: perturbative gravitational scattering meets experimental mathematics*, [2008.09389](#).
- [17] W. D. Goldberger and I. Z. Rothstein, *An Effective field theory of gravity for extended objects*, *Phys. Rev. D* **73** (2006) 104029 [[hep-th/0409156](#)].

- [18] J. Blümlein, A. Maier and P. Marquard, *Five-Loop Static Contribution to the Gravitational Interaction Potential of Two Point Masses*, *Phys. Lett. B* **800** (2020) 135100 [[1902.11180](#)].
- [19] J. Blümlein, A. Maier, P. Marquard and G. Schäfer, *The fifth-order post-Newtonian Hamiltonian dynamics of two-body systems from an effective field theory approach*, *Nucl. Phys. B* **983** (2022) 115900 [[2110.13822](#)].
- [20] J. Blümlein, A. Maier, P. Marquard and G. Schäfer, *Gravity in binary systems at the fifth and sixth post-Newtonian order*, *PoS LL2022* (2022) 012 [[2208.04552](#)].
- [21] A. Einstein, *Über Gravitationswellen*, *Sitzungsber. Preuss. Akad. Wiss. Berlin (Math. Phys.)* **1918** (1918) 154.
- [22] W. L. Burke, *GRAVITATIONAL RADIATION DAMPING OF SLOWLY MOVING SYSTEMS CALCULATED USING MATCHED ASYMPTOTIC EXPANSIONS*, *J. Math. Phys.* **12** (1971) 401.
- [23] K. S. Thorne, *Nonradial Pulsation of General-Relativistic Stellar Models.IV. The Weakfield Limit*, *Astrophys. J.* **158** (1969) 997.
- [24] L. Blanchet and T. Damour, *Tail Transported Temporal Correlations in the Dynamics of a Gravitating System*, *Phys. Rev. D* **37** (1988) 1410.
- [25] L. Blanchet and T. Damour, *Hereditary effects in gravitational radiation*, *Phys. Rev. D* **46** (1992) 4304.
- [26] W. D. Goldberger and A. Ross, *Gravitational radiative corrections from effective field theory*, *Phys. Rev. D* **81** (2010) 124015 [[0912.4254](#)].
- [27] C. R. Galley, A. K. Leibovich, R. A. Porto and A. Ross, *Tail effect in gravitational radiation reaction: Time nonlocality and renormalization group evolution*, *Phys. Rev. D* **93** (2016) 124010 [[1511.07379](#)].
- [28] S. Foffa and R. Sturani, *Tail terms in gravitational radiation reaction via effective field theory*, *Phys. Rev. D* **87** (2013) 044056 [[1111.5488](#)].
- [29] S. Foffa and R. Sturani, *Hereditary terms at next-to-leading order in two-body gravitational dynamics*, *Phys. Rev. D* **101** (2020) 064033 [[1907.02869](#)].
- [30] L. Blanchet, *Gravitational wave tails of tails*, *Class. Quant. Grav.* **15** (1998) 113 [[gr-qc/9710038](#)].
- [31] T. Marchand, L. Blanchet and G. Faye, *Gravitational-wave tail effects to quartic non-linear order*, *Class. Quant. Grav.* **33** (2016) 244003 [[1607.07601](#)].
- [32] C. Cheung, I. Z. Rothstein and M. P. Solon, *From Scattering Amplitudes to Classical Potentials in the Post-Minkowskian Expansion*, *Phys. Rev. Lett.* **121** (2018) 251101 [[1808.02489](#)].
- [33] Z. Bern, C. Cheung, R. Roiban, C.-H. Shen, M. P. Solon and M. Zeng, *Scattering Amplitudes and the Conservative Hamiltonian for Binary Systems at Third Post-Minkowskian Order*, *Phys. Rev. Lett.* **122** (2019) 201603 [[1901.04424](#)].
- [34] Z. Bern, C. Cheung, R. Roiban, C.-H. Shen, M. P. Solon and M. Zeng, *Black Hole Binary Dynamics from the Double Copy and Effective Theory*, *JHEP* **10** (2019) 206 [[1908.01493](#)].
- [35] Z. Bern, J. Parra-Martinez, R. Roiban, M. S. Ruf, C.-H. Shen, M. P. Solon et al., *Scattering Amplitudes, the Tail Effect, and Conservative Binary Dynamics at $O(G^4)$* , *Phys. Rev. Lett.* **128** (2022) 161103 [[2112.10750](#)].

- [36] G. Mogull, J. Plefka and J. Steinhoff, *Classical black hole scattering from a worldline quantum field theory*, *JHEP* **02** (2021) 048 [[2010.02865](#)].
- [37] G. U. Jakobsen, G. Mogull, J. Plefka and J. Steinhoff, *SUSY in the sky with gravitons*, *JHEP* **01** (2022) 027 [[2109.04465](#)].
- [38] G. U. Jakobsen, G. Mogull, J. Plefka and B. Sauer, *All things retarded: radiation-reaction in worldline quantum field theory*, *JHEP* **10** (2022) 128 [[2207.00569](#)].
- [39] C. Dlapa, G. Kälin, Z. Liu and R. A. Porto, *Conservative Dynamics of Binary Systems at Fourth Post-Minkowskian Order in the Large-Eccentricity Expansion*, *Phys. Rev. Lett.* **128** (2022) 161104 [[2112.11296](#)].
- [40] C. Dlapa, G. Kälin, Z. Liu, J. Neef and R. A. Porto, *Radiation Reaction and Gravitational Waves at Fourth Post-Minkowskian Order*, *Phys. Rev. Lett.* **130** (2023) 101401 [[2210.05541](#)].
- [41] G. Kälin and R. A. Porto, *From boundary data to bound states. Part II. Scattering angle to dynamical invariants (with twist)*, *JHEP* **02** (2020) 120 [[1911.09130](#)].
- [42] G. Kälin and R. A. Porto, *From Boundary Data to Bound States*, *JHEP* **01** (2020) 072 [[1910.03008](#)].
- [43] G. Cho, G. Kälin and R. A. Porto, *From boundary data to bound states. Part III. Radiative effects*, *JHEP* **04** (2022) 154 [[2112.03976](#)].
- [44] P. Di Vecchia, C. Heissenberg, R. Russo and G. Veneziano, *Classical gravitational observables from the Eikonal operator*, *Phys. Lett. B* **843** (2023) 138049 [[2210.12118](#)].
- [45] P. Di Vecchia, C. Heissenberg, R. Russo and G. Veneziano, *The eikonal approach to gravitational scattering and radiation at $\mathcal{O}(G^3)$* , *JHEP* **07** (2021) 169 [[2104.03256](#)].
- [46] A. Buonanno, M. Khalil, D. O’Connell, R. Roiban, M. P. Solon and M. Zeng, *Snowmass White Paper: Gravitational Waves and Scattering Amplitudes*, in *Snowmass 2021*, 4, 2022, [2204.05194](#).
- [47] A. Edison and M. Levi, *A tale of tails through generalized unitarity*, *Phys. Lett. B* **837** (2023) 137634 [[2202.04674](#)].
- [48] Z. Bern, L. J. Dixon, D. C. Dunbar and D. A. Kosower, *One loop n point gauge theory amplitudes, unitarity and collinear limits*, *Nucl. Phys. B* **425** (1994) 217 [[hep-ph/9403226](#)].
- [49] Z. Bern, L. J. Dixon, D. C. Dunbar and D. A. Kosower, *Fusing gauge theory tree amplitudes into loop amplitudes*, *Nucl. Phys. B* **435** (1995) 59 [[hep-ph/9409265](#)].
- [50] R. Britto, F. Cachazo and B. Feng, *Generalized unitarity and one-loop amplitudes in $N=4$ super-Yang-Mills*, *Nucl. Phys. B* **725** (2005) 275 [[hep-th/0412103](#)].
- [51] C. Anastasiou, R. Britto, B. Feng, Z. Kunszt and P. Mastrolia, *D -dimensional unitarity cut method*, *Phys. Lett. B* **645** (2007) 213 [[hep-ph/0609191](#)].
- [52] W. D. Goldberger, A. Ross and I. Z. Rothstein, *Black hole mass dynamics and renormalization group evolution*, *Phys. Rev. D* **89** (2014) 124033 [[1211.6095](#)].
- [53] C. R. Galley, *Classical Mechanics of Nonconservative Systems*, *Phys. Rev. Lett.* **110** (2013) 174301 [[1210.2745](#)].
- [54] C. R. Galley, D. Tsang and L. C. Stein, *The principle of stationary nonconservative action for classical mechanics and field theories*, [1412.3082](#).

- [55] R. Fujita, *Gravitational radiation for extreme mass ratio inspirals to the 14th post-Newtonian order*, *Prog. Theor. Phys.* **127** (2012) 583 [[1104.5615](#)].
- [56] R. Fujita, *Gravitational Waves from a Particle in Circular Orbits around a Schwarzschild Black Hole to the 22nd Post-Newtonian Order*, *Prog. Theor. Phys.* **128** (2012) 971 [[1211.5535](#)].
- [57] R. A. Porto, *The effective field theorist's approach to gravitational dynamics*, *Phys. Rept.* **633** (2016) 1 [[1601.04914](#)].
- [58] M. Levi, *Effective Field Theories of Post-Newtonian Gravity: A comprehensive review*, *Rept. Prog. Phys.* **83** (2020) 075901 [[1807.01699](#)].
- [59] R. A. Porto, *Post-Newtonian corrections to the motion of spinning bodies in NRGR*, *Phys. Rev. D* **73** (2006) 104031 [[gr-qc/0511061](#)].
- [60] R. A. Porto and I. Z. Rothstein, *Spin(1)Spin(2) Effects in the Motion of Inspiralling Compact Binaries at Third Order in the Post-Newtonian Expansion*, *Phys. Rev. D* **78** (2008) 044012 [[0802.0720](#)].
- [61] R. A. Porto and I. Z. Rothstein, *Next to Leading Order Spin(1)Spin(1) Effects in the Motion of Inspiralling Compact Binaries*, *Phys. Rev. D* **78** (2008) 044013 [[0804.0260](#)].
- [62] R. A. Porto, *Absorption effects due to spin in the worldline approach to black hole dynamics*, *Phys. Rev. D* **77** (2008) 064026 [[0710.5150](#)].
- [63] M. Levi, *Next to Leading Order gravitational Spin-Orbit coupling in an Effective Field Theory approach*, *Phys. Rev. D* **82** (2010) 104004 [[1006.4139](#)].
- [64] M. Levi, *Next to Leading Order gravitational Spin1-Spin2 coupling with Kaluza-Klein reduction*, *Phys. Rev. D* **82** (2010) 064029 [[0802.1508](#)].
- [65] B. Kol, M. Levi and M. Smolkin, *Comparing space+time decompositions in the post-Newtonian limit*, *Class. Quant. Grav.* **28** (2011) 145021 [[1011.6024](#)].
- [66] M. Levi, *Binary dynamics from spin1-spin2 coupling at fourth post-Newtonian order*, *Phys. Rev. D* **85** (2012) 064043 [[1107.4322](#)].
- [67] M. Levi and J. Steinhoff, *Equivalence of ADM Hamiltonian and Effective Field Theory approaches at next-to-next-to-leading order spin1-spin2 coupling of binary inspirals*, *JCAP* **12** (2014) 003 [[1408.5762](#)].
- [68] M. Levi and J. Steinhoff, *Spinning gravitating objects in the effective field theory in the post-Newtonian scheme*, *JHEP* **09** (2015) 219 [[1501.04956](#)].
- [69] M. Levi and J. Steinhoff, *Leading order finite size effects with spins for inspiralling compact binaries*, *JHEP* **06** (2015) 059 [[1410.2601](#)].
- [70] M. Levi and J. Steinhoff, *Complete conservative dynamics for inspiralling compact binaries with spins at the fourth post-Newtonian order*, *JCAP* **09** (2021) 029 [[1607.04252](#)].
- [71] M. Levi and J. Steinhoff, *Next-to-next-to-leading order gravitational spin-orbit coupling via the effective field theory for spinning objects in the post-Newtonian scheme*, *JCAP* **01** (2016) 011 [[1506.05056](#)].
- [72] M. Levi and J. Steinhoff, *Next-to-next-to-leading order gravitational spin-squared potential via the effective field theory for spinning objects in the post-Newtonian scheme*, *JCAP* **01** (2016) 008 [[1506.05794](#)].

- [73] M. Levi and J. Steinhoff, *EFTofPNG: A package for high precision computation with the Effective Field Theory of Post-Newtonian Gravity*, *Class. Quant. Grav.* **34** (2017) 244001 [[1705.06309](#)].
- [74] N. T. Maia, C. R. Galley, A. K. Leibovich and R. A. Porto, *Radiation reaction for spinning bodies in effective field theory I: Spin-orbit effects*, *Phys. Rev. D* **96** (2017) 084064 [[1705.07934](#)].
- [75] N. T. Maia, C. R. Galley, A. K. Leibovich and R. A. Porto, *Radiation reaction for spinning bodies in effective field theory II: Spin-spin effects*, *Phys. Rev. D* **96** (2017) 084065 [[1705.07938](#)].
- [76] M. Levi, S. Mougiakakos and M. Vieira, *Gravitational cubic-in-spin interaction at the next-to-leading post-Newtonian order*, [1912.06276](#).
- [77] M. Levi and F. Teng, *NLO gravitational quartic-in-spin interaction*, *JHEP* **01** (2021) 066 [[2008.12280](#)].
- [78] M. Levi, A. J. Mcleod and M. Von Hippel, *N^3LO gravitational spin-orbit coupling at order G^4* , *JHEP* **07** (2021) 115 [[2003.02827](#)].
- [79] M. Levi, A. J. Mcleod and M. Von Hippel, *N^3LO gravitational quadratic-in-spin interactions at G^4* , *JHEP* **07** (2021) 116 [[2003.07890](#)].
- [80] J.-W. Kim, M. Levi and Z. Yin, *Quadratic-in-spin interactions at fifth post-Newtonian order probe new physics*, *Phys. Lett. B* **834** (2022) 137410 [[2112.01509](#)].
- [81] J.-W. Kim, M. Levi and Z. Yin, *N^3LO spin-orbit interaction via the EFT of spinning gravitating objects*, *JHEP* **05** (2023) 184 [[2208.14949](#)].
- [82] J.-W. Kim, M. Levi and Z. Yin, *N^3LO quadratic-in-spin interactions for generic compact binaries*, *JHEP* **03** (2023) 098 [[2209.09235](#)].
- [83] M. Levi, R. Morales and Z. Yin, *From the EFT of spinning gravitating objects to Poincaré and gauge invariance at the 4.5PN precision frontier*, *JHEP* **09** (2023) 090 [[2210.17538](#)].
- [84] M. Levi and Z. Yin, *Completing the fifth PN precision frontier via the EFT of spinning gravitating objects*, *JHEP* **04** (2023) 079 [[2211.14018](#)].
- [85] A. Ross, *Multipole expansion at the level of the action*, *Phys. Rev. D* **85** (2012) 125033 [[1202.4750](#)].
- [86] P. Jaranowski and G. Schafer, *Towards the 4th post-Newtonian Hamiltonian for two-point-mass systems*, *Phys. Rev. D* **86** (2012) 061503 [[1207.5448](#)].
- [87] D. Bini and A. Geralico, *Higher-order tail contributions to the energy and angular momentum fluxes in a two-body scattering process*, *Phys. Rev. D* **104** (2021) 104020 [[2108.05445](#)].
- [88] C. R. Galley and M. Tiglio, *Radiation reaction and gravitational waves in the effective field theory approach*, *Phys. Rev. D* **79** (2009) 124027 [[0903.1122](#)].
- [89] C. R. Galley and A. K. Leibovich, *Radiation reaction at 3.5 post-Newtonian order in effective field theory*, *Phys. Rev. D* **86** (2012) 044029 [[1205.3842](#)].
- [90] L. Blanchet, S. Foffa, F. Larrouturou and R. Sturani, *Logarithmic tail contributions to the energy function of circular compact binaries*, *Phys. Rev. D* **101** (2020) 084045 [[1912.12359](#)].

- [91] G. L. Almeida, S. Foffa and R. Sturani, *Tail contributions to gravitational conservative dynamics*, *Phys. Rev. D* **104** (2021) 124075 [[2110.14146](#)].
- [92] L. Kadanoff and G. Baym, *Quantum Statistical Mechanics: Green's Function Methods in Equilibrium and Nonequilibrium Problems*, Frontiers in Physics. A Lecture Note and Reprint Series. W.A. Benjamin, 1962.
- [93] L. V. Keldysh, *Diagram technique for nonequilibrium processes*, *Zh. Eksp. Teor. Fiz.* **47** (1964) 1515.
- [94] H. Elvang and Y.-t. Huang, *Scattering Amplitudes*, [1308.1697](#).
- [95] H. Elvang and Y.-t. Huang, *Scattering Amplitudes in Gauge Theory and Gravity*. Cambridge University Press, 4, 2015.
- [96] L. J. Dixon, *A brief introduction to modern amplitude methods*, in *Theoretical Advanced Study Institute in Elementary Particle Physics: Particle Physics: The Higgs Boson and Beyond*, pp. 31–67, 2014, [1310.5353](#), DOI.
- [97] J. J. M. Carrasco, *Gauge and Gravity Amplitude Relations*, in *Theoretical Advanced Study Institute in Elementary Particle Physics: Journeys Through the Precision Frontier: Amplitudes for Colliders*, pp. 477–557, WSP, 2015, [1506.00974](#), DOI.
- [98] Z. Bern, S. Davies and J. Nohle, *Double-Copy Constructions and Unitarity Cuts*, *Phys. Rev. D* **93** (2016) 105015 [[1510.03448](#)].
- [99] J. L. Bourjaily, E. Herrmann and J. Trnka, *Prescriptive Unitarity*, *JHEP* **06** (2017) 059 [[1704.05460](#)].
- [100] J. J. M. Carrasco and H. Johansson, *Generic multiloop methods and application to $\mathcal{N} = 4$ super-Yang-Mills*, *J. Phys.* **A44** (2011) 454004 [[1103.3298](#)].
- [101] J. J. M. Carrasco and H. Johansson, *Five-point amplitudes in $\mathcal{N} = 4$ super-Yang-Mills theory and $\mathcal{N} = 8$ supergravity*, *Phys. Rev.* **D85** (2012) 025006 [[1106.4711](#)].
- [102] Z. Bern, J. J. M. Carrasco, L. J. Dixon, H. Johansson and R. Roiban, *Simplifying Multiloop Integrands and Ultraviolet Divergences of Gauge Theory and Gravity Amplitudes*, *Phys. Rev. D* **85** (2012) 105014 [[1201.5366](#)].
- [103] Z. Bern, J. J. Carrasco, M. Chiodaroli, H. Johansson and R. Roiban, *The Duality Between Color and Kinematics and its Applications*, [1909.01358](#).
- [104] A. Edison, S. He, H. Johansson, O. Schlotterer, F. Teng and Y. Zhang, *Perfecting one-loop BCJ numerators in SYM and supergravity*, *JHEP* **02** (2023) 164 [[2211.00638](#)].
- [105] A. Edison and M. Tegevi, *Color-kinematics dual representations of one-loop matrix elements in the open-superstring effective action*, *JHEP* **10** (2023) 022 [[2210.14865](#)].
- [106] J. J. M. Carrasco and N. H. Pavao, *Even-point Multi-loop Unitarity and its Applications: Exponentiation, Anomalies and Evanescence*, [2307.16812](#).
- [107] N. Arkani-Hamed and J. Trnka, *The Amplituhedron*, *JHEP* **10** (2014) 030 [[1312.2007](#)].
- [108] Z. Bern, J. J. M. Carrasco and H. Johansson, *New Relations for Gauge-Theory Amplitudes*, *Phys. Rev. D* **78** (2008) 085011 [[0805.3993](#)].
- [109] Z. Bern, T. Dennen, Y.-t. Huang and M. Kiermaier, *Gravity as the Square of Gauge Theory*, *Phys. Rev. D* **82** (2010) 065003 [[1004.0693](#)].

- [110] Z. Bern, J. J. M. Carrasco and H. Johansson, *Perturbative Quantum Gravity as a Double Copy of Gauge Theory*, *Phys. Rev. Lett.* **105** (2010) 061602 [[1004.0476](#)].
- [111] R. Britto, F. Cachazo and B. Feng, *New recursion relations for tree amplitudes of gluons*, *Nucl. Phys. B* **715** (2005) 499 [[hep-th/0412308](#)].
- [112] R. Britto, F. Cachazo, B. Feng and E. Witten, *Direct proof of tree-level recursion relation in Yang-Mills theory*, *Phys. Rev. Lett.* **94** (2005) 181602 [[hep-th/0501052](#)].
- [113] N. Arkani-Hamed, J. Bourjaily, F. Cachazo and J. Trnka, *Local Spacetime Physics from the Grassmannian*, *JHEP* **01** (2011) 108 [[0912.3249](#)].
- [114] N. Arkani-Hamed, J. L. Bourjaily, F. Cachazo, A. B. Goncharov, A. Postnikov and J. Trnka, *Grassmannian Geometry of Scattering Amplitudes*. Cambridge University Press, 4, 2016, [10.1017/CBO9781316091548](#), [[1212.5605](#)].
- [115] N. Arkani-Hamed, T.-C. Huang and Y.-t. Huang, *Scattering amplitudes for all masses and spins*, *JHEP* **11** (2021) 070 [[1709.04891](#)].
- [116] M.-Z. Chung, Y.-T. Huang, J.-W. Kim and S. Lee, *The simplest massive S-matrix: from minimal coupling to Black Holes*, *JHEP* **04** (2019) 156 [[1812.08752](#)].
- [117] P. H. Damgaard, K. Haddad and A. Helset, *Heavy Black Hole Effective Theory*, *JHEP* **11** (2019) 070 [[1908.10308](#)].
- [118] R. Aoude, K. Haddad and A. Helset, *On-shell heavy particle effective theories*, *JHEP* **05** (2020) 051 [[2001.09164](#)].
- [119] F. Cachazo, S. He and E. Y. Yuan, *Scattering of Massless Particles: Scalars, Gluons and Gravitons*, *JHEP* **07** (2014) 033 [[1309.0885](#)].
- [120] F. Cachazo, S. He and E. Y. Yuan, *Scattering of Massless Particles in Arbitrary Dimensions*, *Phys. Rev. Lett.* **113** (2014) 171601 [[1307.2199](#)].
- [121] A. Edison and F. Teng, *Efficient Calculation of Crossing Symmetric BCJ Tree Numerators*, *JHEP* **12** (2020) 138 [[2005.03638](#)].
- [122] G. Passarino and M. J. G. Veltman, *One Loop Corrections for $e^+ e^-$ Annihilation Into $\mu^+ \mu^-$ in the Weinberg Model*, *Nucl. Phys. B* **160** (1979) 151.
- [123] S. Laporta and E. Remiddi, *The Analytical value of the electron ($g-2$) at order α^{**3} in QED*, *Phys. Lett. B* **379** (1996) 283 [[hep-ph/9602417](#)].
- [124] V. A. Smirnov, *Feynman integral calculus*. Springer, Berlin, Heidelberg, 2006.
- [125] V. A. Smirnov, *Analytic tools for Feynman integrals*, vol. 250. 2012, [10.1007/978-3-642-34886-0](#).
- [126] W. L. van Neerven and J. A. M. Vermaseren, *LARGE LOOP INTEGRALS*, *Phys. Lett. B* **137** (1984) 241.
- [127] Z. Bern, L. J. Dixon and D. A. Kosower, *Dimensionally regulated one loop integrals*, *Phys. Lett. B* **302** (1993) 299 [[hep-ph/9212308](#)].
- [128] Z. Bern, L. J. Dixon and D. A. Kosower, *Dimensionally regulated pentagon integrals*, *Nucl. Phys. B* **412** (1994) 751 [[hep-ph/9306240](#)].
- [129] L. M. Brown and R. P. Feynman, *Radiative corrections to Compton scattering*, *Phys. Rev.* **85** (1952) 231.

- [130] G. 't Hooft and M. J. G. Veltman, *Scalar One Loop Integrals*, [*Nucl. Phys. B* **153** \(1979\) 365](#).
- [131] R. Britto and B. Feng, *Integral coefficients for one-loop amplitudes*, [*JHEP* **02** \(2008\) 095](#) [[0711.4284](#)].
- [132] G. Ossola, C. G. Papadopoulos and R. Pittau, *Reducing full one-loop amplitudes to scalar integrals at the integrand level*, [*Nucl. Phys. B* **763** \(2007\) 147](#) [[hep-ph/0609007](#)].
- [133] D. Forde, *Direct extraction of one-loop integral coefficients*, [*Phys. Rev. D* **75** \(2007\) 125019](#) [[0704.1835](#)].
- [134] D. Kosmopoulos, *Simplifying D-dimensional physical-state sums in gauge theory and gravity*, [*Phys. Rev. D* **105** \(2022\) 056025](#) [[2009.00141](#)].
- [135] E. Gardi, S. Abreu, R. Britto, C. Duhr and J. Matthew, *The diagrammatic coaction*, [*PoS LL2022* \(2022\) 015](#) [[2207.07843](#)].
- [136] H. Frellesvig, F. Gasparotto, S. Laporta, M. K. Mandal, P. Mastrolia, L. Mattiazzi et al., *Decomposition of Feynman Integrals by Multivariate Intersection Numbers*, [*JHEP* **03** \(2021\) 027](#) [[2008.04823](#)].
- [137] D. A. Kosower, B. Maybee and D. O'Connell, *Amplitudes, Observables, and Classical Scattering*, [*JHEP* **02** \(2019\) 137](#) [[1811.10950](#)].
- [138] A. Herderschee, R. Roiban and F. Teng, *The sub-leading scattering waveform from amplitudes*, [*JHEP* **06** \(2023\) 004](#) [[2303.06112](#)].
- [139] B. R. Holstein and A. Ross, *Spin Effects in Long Range Gravitational Scattering*, [0802.0716](#).
- [140] V. Vaidya, *Gravitational spin Hamiltonians from the S matrix*, [*Phys. Rev. D* **91** \(2015\) 024017](#) [[1410.5348](#)].
- [141] G. L. Almeida, A. Müller, S. Foffa and R. Sturani, *Conservative binary dynamics from gravitational tail emission processes*, [2307.05327](#).
- [142] W. D. Goldberger and I. Z. Rothstein, *Dissipative effects in the worldline approach to black hole dynamics*, [*Phys. Rev. D* **73** \(2006\) 104030](#) [[hep-th/0511133](#)].
- [143] A. Brandhuber, G. Chen, G. Travaglini and C. Wen, *A new gauge-invariant double copy for heavy-mass effective theory*, [*JHEP* **07** \(2021\) 047](#) [[2104.11206](#)].
- [144] C. Galley, *Radiation reaction and self-force in curved spacetime in a field theory approach*, Ph.D. thesis, Maryland U., 11, 2007.
- [145] A. V. Smirnov and F. S. Chuharev, *FIRE6: Feynman Integral REDuction with Modular Arithmetic*, [*Comput. Phys. Commun.* **247** \(2020\) 106877](#) [[1901.07808](#)].
- [146] L. Blanchet, *Time asymmetric structure of gravitational radiation*, [*Phys. Rev. D* **47** \(1993\) 4392](#).
- [147] Z. Bern, H.-H. Chi, L. Dixon and A. Edison, *Two-Loop Renormalization of Quantum Gravity Simplified*, [*Phys. Rev. D* **95** \(2017\) 046013](#) [[1701.02422](#)].
- [148] L. Blanchet, *Quadrupole-quadrupole gravitational waves*, [*Class. Quant. Grav.* **15** \(1998\) 89](#) [[gr-qc/9710037](#)].
- [149] L. Blanchet, B. R. Iyer and B. Joguet, *Gravitational waves from inspiralling compact*

binaries: Energy flux to third postNewtonian order, *Phys. Rev. D* **65** (2002) 064005 [gr-qc/0105098].

- [150] Q. Henry and F. Larrouturou, *Conservative tail and failed-tail effects at the fifth post-Newtonian order*, *Phys. Rev. D* **108** (2023) 084048 [2307.05860].
- [151] D. Gerosa and M. Vallisneri, *filltex: Automatic queries to ADS and INSPIRE databases to fill LaTeX bibliography*, *The Journal of Open Source Software* **2** (2017) 222.
- [152] X. Liu and Y.-Q. Ma, *AMFlow: A Mathematica package for Feynman integrals computation via auxiliary mass flow*, *Comput. Phys. Commun.* **283** (2023) 108565 [2201.11669].
- [153] J. Klappert, F. Lange, P. Maierhöfer and J. Usovitsch, *Integral reduction with Kira 2.0 and finite field methods*, *Comput. Phys. Commun.* **266** (2021) 108024 [2008.06494].
- [154] D. H. Bailey and D. J. Broadhurst, *Parallel integer relation detection: Techniques and applications*, *Math. Comput.* **70** (2001) 1719 [math/9905048].
- [155] A. Smirnov. <https://gitlab.com/feynmanintegrals/pslq>.